Effect of vehicular traffic, remote sources and new particle formation on the activation properties of cloud condensation nuclei in the megacity of São Paulo, Brazil

Carlos Eduardo Souto-Oliveira[1,2], Maria de Fátima Andrade[3], Prashant Kumar[4,5], Fábio Juliano da Silva Lopes[3,6], Marly Babinski[1], Eduardo Landulfo[6].

[1]Geochronological Research Centre, Institute of Geosciences, University of São Paulo, São Paulo, 05508-080, Brazil
[2]Chemistry Research Centre, UNIFIEO, São Paulo, 06018-903, Brazil
[3]Department of Atmospheric Sciences, Institute of Astronomy, Geophysics and Atmospheric Sciences, University of São Paulo, São Paulo, 05508-090, Brazil
[4]Department of Civil and Environmental Engineering, Faculty of Engineering and Physical Sciences (FEPS), University of Surrey, GuilfordGU2 7XH, United Kingdom
[5]Environmental Flow (EnFlo) Research Centre, Faculty of Engineering and Physical Sciences (FEPS), University of Surrey, GuildfordGU2 7XH, United Kingdom
[6]Nuclear and Energy Research Institute, IPEN-CNEN, Centre for Laser and Applications (CLA), São Paulo, 05508-970, Brazil

Correspondence to: Carlos Eduardo Souto-Oliveira (carlos.edu.oliveira@usp.br)

Abstract. Atmospheric aerosol is the primary source of cloud condensation nuclei (CCN). The microphysics and chemical composition of aerosols can affect cloud development and the precipitation process. Among studies conducted in Latin America, only a handful have reported the impact of urban aerosol on CCN activation parameters such as activation ratio (AR) and activation diameter (D_{act}). With over 20 million inhabitants, the Metropolitan Area of São Paulo (MASP) is the largest megacity in South America. To our knowledge, this is the first study to assess the impact that remote sources and new particle formation (NPF) events have on CCN activation properties in a South American megacity. The measurements were conducted in the MASP between August and September 2014. We measured the CCN within the 0.2–1.0% range of supersaturation, together with particle number concentration (PNC) and particle number distribution (PND), as well as trace-element concentrations and black carbon (BC). NPF events were identified on 35% of the sampling days. Combining multivariate analysis in the form of positive matrix factorization (PMF) with an aerosol profile from lidar and HYSPLIT model analyses, allowed us to identify the main contribution of vehicular traffic in all days and sea-salt and biomass-burning from remote regions on 28% and 21% of the sampling days, respectively. The AR and D_{act} parameters showed distinct patterns for daytime with intense vehicular traffic and nighttime periods. For example,

CCN activation was lower during the daytime than during the nighttime periods, a pattern that was found to be associated mainly with local road traffic emissions. A decrease in CCN activation was observed on the NPF event days, mainly due to high concentrations of particles with smaller diameters. We also found that aerosols from sea-salt + industrial emissions and vehicular emissions + biomass-burning had minor effects on D_{act}. For example, nights with biomass burning + vehicular emissions showed slightly lower CCN activation properties than did sea-salt + industrial and non-event nights. Our results show that particulate matter from local vehicular emissions during the daytime has a greater effect on CCN activation parameters than does that from remote sources.

1 Introduction

Atmospheric aerosol has been the focus of numerous studies, because of its adverse effects on public health and climate (Heal et al., 2012). Aerosol particles are a significant source of cloud condensation nuclei (CCN). Owing to their microphysics and chemical composition, aerosol particles can affect cloud development and the precipitation process. The high concentrations of CCN in the air favour the formation of clouds with small droplets, which can lead to suppression of precipitation in shallow and short-lived clouds (Andreae and Rosenfeld, 2008). Such phenomena have been observed at different places. A study carried out in the Brazilian Amazon showed a reduction in precipitation during biomass-burning events, due to greater scavenging from smoky clouds than from clouds formed under clean (blue and green ocean) air masses. The smoky clouds were shown to form at higher altitudes (> 4 km), due to their smaller droplet size, and to produce hydrometeors including isolated intense showers and thunderstorms (Andreae et al., 2004; Freud et al., 2008).

The CCN activation properties can be estimated by parameters such as activation ratio (AR) and activation diameter (D_{act}). In several studies representing different locations of the world, these parameters have been employed for determining the efficiency of aerosol particles in acting as CCN. The variability of these parameters is dependent on size and chemical composition of particles. In general, D_{act} is more sensitive to the chemical composition of aerosols, whereas the AR is related to particle size and chemical composition. Large particles, inorganic salts and polar organic molecules are typically more hygroscopic than are smaller particles and non-polar molecules (e.g. hydrocarbons). Some studies have reported that aerosol from air masses containing pollutants (e.g. urban, fresh traffic and biomass-burning emissions) are less efficient in activating CCN (>D_{act} and <AR) than are non-polluted (e.g. forest and marine) air masses (Frank et al., 2006; Andreae and Rosenfeld, 2008; Quinn et al., 2008; Furutani et al., 2008; Bulkart et al., 2011; Deng et al., 2013; Leng et al., 2013; Paramonov et al., 2013). However, studies carried out at different locations and under different environmental conditions have demonstrated that aged polluted aerosols present CCN activation properties similar to those of non-polluted or even marine environment air (Peng et al., 2014). Those observations are supported by the growth of particles, atmospheric processing of non-soluble organics and mixture with more hygroscopic compounds such as sulphate, nitrate and organic acids (Andreae et al., 2004; McFiggans et al., 2006; Quinn et al., 2008; Furutani et al., 2008; Dusek et al., 2010; Bougiatioti et al., 2011; Zhang et al.,

2014).

Aerosols originate from primary and secondary processes. Primary aerosols are emitted into the atmosphere directly by anthropogenic and natural sources. In contrast, secondary aerosols are formed in the atmosphere through the nucleation of no- or low-volatile gases containing inorganic and organic compounds, followed by growth to larger particles (Holmes, 2007). New particle formation (NPF) directly affects particle number concentration (PNC), particle size distribution (PND) and the optical properties of aerosols, as well as the properties of CCN and clouds. These events have been recently studied in urban, coastal and forest environments (Kulmala et al., 2004; Dal Maso et al., 2005; Backman et al., 2012; Betha et al., 2013; Peng et al., 2014; Nie et al., 2014; An et al., 2015; Sorribas et al., 2015; Kumar et al., 2014). However, there have been only a few studies evaluating the effect of NPF on CCN properties (Dusek et al., 2010; Yue et al., 2011; Sihto et al., 2011; Paramonov et al., 2013).

Typically, nucleation events occur in clean air under high solar radiation conditions. Many authors have shown that sulphuric acid and precursor species (SO_2, hydroxyl, NH_3 and oxidised organic compounds) play important roles in the nucleation process (Yue et al., 2011; Andreae, 2013; Long et al., 2016). Reche et al. (2011) suggested that the occurrence of SO_2 peaks contributes to midday nucleation bursts as a function of the sources. Kumar et al. (2014) discussed the different conditions for the secondary formation of particles over different types of urban areas. Recent studies have demonstrated the importance of oxidised organic vapours to drive NPF nucleation with H_2SO_4 and enhance secondary particle growth (Metzger et al., 2010; Donahue et al., 2013). Zhu et al. (2014) demonstrated the importance of secondary organic aerosols (SOAs) to particle growth over urban sites with different levels of pollution.

Volatile organic compounds (VOCs) constitute a fundamental precursor of SOAs and tropospheric ozone (O_3). Primary organic aerosols originate from biogenic sources (isoprene, terpenes, dimethyl sulphide and dicarboxylic acids) and anthropogenic sources (biomass burning and traffic), thereafter being emitted directly into the atmosphere. Atmospheric species such as hydroxyl radicals and O_3 play a major role in VOC chemical degradation and the consequent formation of SOAs, which contain polar oxygenated functional groups (Hallquist et al., 2009). Recent studies have confirmed that the SOA yield is dependent on high concentrations of nitrogen oxides (NO_x), which explain the formation of certain SOAs, such as those derived from isoprene degradation (Shilling et al., 2013; Yuan et al., 2013). Another study, carried out in California, showed that vehicular emissions play an important role in the formation of urban SOAs (Ortega et al., 2016). In MASP, biofuels (ethanol and biodiesel) increase the emission of carbonyl compounds, which can be precursors of secondary oxygenated pollutants. In one study conducted in the MASP, Oyama et al. (2015) showed the emission factors for light-duty vehicles, which run on gasohol or ethanol, and for heavy-duty vehicles, which run on biodiesel. The authors found that oxygenated hydrocarbon compounds accounted for a major proportion of the aerosol composition. Those same authors also reported that, during biodiesel combustion, heavy-duty vehicles in the MASP emit greater quantities of volatile nitrogen compounds, which are associated with the NO_x chemistry, than light-duty vehicles in the MASP. Wallington et al. (2016) showed that engine calibration is a determinant of NO_x emissions, which are higher from biodiesel-burning vehicles. The use of biofuels has introduced new challenges for the description of atmospheric chemistry, by increasing the emissions of

carbonyl and polycyclic aromatic hydrocarbons (PAHs, including those containing nitrogen and those that are oxygenated), as shown by Karavalakis et al. (2011).

With over 20 million inhabitants, the MASP is the biggest megacity in South America. Therefore, the MASP represents an important city for global-scale atmospheric studies. The MASP fleet comprises more than 7 million vehicles, which constitute one of the main sources of particles, together with a variety of industries and construction activities (IBGE, 2014). To date, there has been only one study measuring and modelling CCN in the MASP (Almeida et al., 2014). In general, there has been a limited number of studies reporting CCN, PNC and PND measurements, comparing Latin American cities with those in Europe and United States in terms of the effects that those properties have on the atmosphere (IPCC,2013).

The aim of this study was to evaluate CCN activation properties under the influence of local and remote sources, as well as to identify NPF events. We measured CCN simultaneously with PNC, PND, black carbon (BC) and trace-elements. PND contour plots were constructed in order to identify and classify NPF events. Light detection and ranging (lidar) analyses and Hybrid Single Particle Lagrangian Integrated Trajectory (HYSPLIT) analyses (Draxler and Rolph, 2003) were combined with multivariate analysis in the form of positive matrix factorization (PMF) in order to identify air masses from remote sources in the MASP. We evaluated the effects that those air masses associate with local sources and NPF events had on CCN activation properties. To our knowledge, this is the first study evaluating the effects of remote sources and NPF events on CCN activation properties in a megacity in South America.

2 Methodology

2.1 Site description and meteorological data

The SPMA (23.5°S; 46.6°W) is an urban region encompassing an area of 7946 km^2, in the south-western region of Brazil (Fig. 1). With over 20 million inhabitants, the MASP is the largest megacity in South America and rank among the ten most populous in the world. The MASP is situated in a sedimentary basin within the state of São Paulo (the Tietê River valley, which has a mean elevation of 720 m), approximately 45 km north-west of the Atlantic Ocean.

The measurements were taken on the rooftop of the *Instituto de Astronomia, Geofísica e Ciências Atmosféricas* (IAG, Institute of Astronomy, Geophysics and Atmospheric Sciences) on the main campus of the University of São Paulo (USP, 23.56°S; 46.73°W), which is situated in the western region of the city. There are two main roads (the Marginal Pinheiros and the Marginal Tietê),approximately1 km northeast and 4 km north of the sampling site, respectively. During the daytime period (0700–1900 h, local time), those roads have a high mean hourly traffic density (8000 automobiles, 1500 motorcycles, 220 trucks and 90 buses). At night, traffic volume is less than half of what is noted during the day and is dominated by heavy-duty vehicles (mainly trucks), which are not allowed to circulate during the daytime hours. Other important sources of particles in the MASP are construction sites on and near the USP campus and a cement industry about 2 km to the west. The major industrial areas (Mauá and Cubatão) are respectively located approximately 30 and 45 km to the south-east, the industrial city of Cubatão being located in the coastal region (Fig. 1).

2.2 Measurements of CCN

The CCN were counted in a single-column continuous-flow stream-wise thermal gradient chamber (CCN-100; Droplet Measurement Technologies, Boulder, CO, USA). The supersaturated water vapor is generated inside the column centre line (radius, 0.9 mm; length, 360 mm; and wall thickness, 8 mm), which is controlled by the gradient temperature. When the supersaturation (SS) generated is greater than the critical SS, the particle grows to the critical D_{act}, after which it has the potential to become a cloud droplet. As the activated particles leave the column chamber, those in the 0.75–10 µm size range are counted by an optical particle counter, which employs (OPC) a standard light scattering technique (Roberts and Nenes, 2005).

All samples were collected between 19 August and 3 September 2014. The CCN counter was operated at a flow rate of 0.5 L min^{-1} with variable supersaturation (0.2, 0.4, 0.6, 0.8 and 1.0%). Each cycle (~25 min) corresponds to measurements of all supersaturation, each supersaturation being measured during 5-min; our analysis considered only the data for steady-states upper saturation.

2.3 Measurements of size-resolved particles

The PND and PNC were measured with a scanning mobility particle sizer (SMPS, model3936; TSI Inc., St. Paul, MN, USA). The SMPS consists of a differential mobility analyser (DMA, model 3080; TSI Inc.) and a condensation particle counter (CPC, model 3010; TSI Inc.). The DMA separates particles according to their electrical mobility, and the particles that pass through the DMA column are counted by the CPC (Kumar et al., 2010). In the CPC, particles grow into droplets by condensation of alcohol vapour and are then counted by a laser beam.

The aerosol size distribution was measured in the 10–450 nm range, particles being scanned in 22 diameter size bins, with a 5-min time resolution. The gas sample and sheath flow rate were 1.0 and 6.0 L min^{-1}, respectively. Determining PNCs from the SMPS has been found to result in the undercounting of particles during ambient measurements, mainly due to lower DMA transfer probability or deviation in sampling and sheath flow rates (Almeida et al., 2014). Another deviation is related to the different diameter size range of particles measured by the SMPS (10–450 nm) and CCN (<10 µm), which can lead to overestimation of AR values, as calculated from the CCN/PNC ratio. A correction factor of 1.3 was applied to the entire data set in order to correct for undercounting during the measurement of PNCs and for overestimation of the AR. That factor was obtained by linear fitting of scatterplot data (CCN versus PNC) with AR values >1.

2.4 Measurements of BC and trace-element species and positive matrix factorisation analysis

A Micro-orifice Uniform Deposit Impactor (MOUDI) was used in order to collect particles measuring <0.056, 0.05618, 0.1, 0.18, 0.32, 0.56, 1.0, 1.8, 3.2, 5.6 and 10 µm. The MOUDI selects particles by the size of its orifices and operates with a sampling air flow of 30 L min^{-1}. In each stage, the particles larger than the size of micro-orifice were collected on polycarbonate filters (Whatman, 47 mm diameter, 8 µm pore size). The sampling intervals were 12h (0700–1900h and 1900–

0700h, local time). After the sampling, the filters were stored in a temperature- and humidity-controlled room for subsequent analysis.

The aerosol mass concentrations were determined gravimetrically before and after the sampling; the filters were weighed on a microbalance with a 1 µg readability (Mettler-Toledo, Columbus, OH, USA). Elemental concentrations were determined by Energy Dispersive X-ray Fluorescence Spectrometer (EDX 700; Shimadzu Corporation, Analytical Instruments Division, Tokyo, Japan). The spectrometer operates at 5–50 kV and 1–1,000 µA, using a low-power Rh-target tube, and the elemental characteristic X-ray radiation emitted from the aerosol sample is detected with an Si(Li) detector. The spectra obtained were processed and quantified with the Win-QXAS program, available from the International Atomic Energy Agency (http://www. iaea.org/OurWork/ST/NA/NAAL/pci/ins/xrf/pciXRFdown.php). We measured BC by optical reflectance with a smoke stain reflectometer (model 43D; Diffusion Systems Ltd, London, UK). Visible light was emitted from a tungsten lamp, and the reflected radiation was detected. The empirical calibration curve that converts the reflected signal to BC concentrations was obtained. The light absorption by the carbonaceous fraction present in atmospheric aerosol is correlated with elemental carbon.

Source apportionment analyses were performed using the PMF model (version 5.0), an operational system from the United States Environmental Protection Agency. The analysis was performed for total concentrations of trace-elements and BC and for average CO concentrations. The number of factors (n=4) was adjusted to obtain the best $Q_{theory} \approx Q_{robust}$ and physical validity of the model. Estimation of the goodness of the model fit was achieved by minimal values of Q and a scaled residual between −2 and +2, following the recommendations of Reff et al. (2007)

2.5 Monitoring of gases and ultraviolet radiation

To determine the importance of the concentrations of certain gases (SO_2, O_3, NO, CO and NO_x) and ultraviolet (UV) radiation on NPF event days, we considered the hourly values of the compounds measured at air quality stations operated by the São Paulo State *Companhia de Tecnologia de Saneamento Ambiental* (CETESB, Environmental Protection Agency). The O_3 and UV radiation were measured at a CETESB station on the USP campus, approximately 500m from the IAG. The SO_2, O_3, NO and NO_x data were obtained from four CETESB stations located off of the USP campus: 7 km to the north-west (Osasco); 5 km to the north (Marginal Pinheiros); 10 km to the south-east (Congonhas); and 5 km to the south-west (Taboão da Serra). Those four stations were chosen in order to represent the influence of wind direction on the behaviour of the particulate matter concentrations.

2.6 Lidar and trajectory analyses

A Raman lidar system installed at the Brazilian Nuclear and Energy Research Institute, designated Lidar do Município de São Paulo I (MSP-Lidar I, lidar I of the Municipality of São Paulo), approximately 400 m from the IAG site, was employed in order to take independent measurements related to particle extinction profiles and backscatter coefficients, thus determining the particle extinction-to-backscatter ratio, at 532 and 355 nm, respectively. The MSP-Lidar I system belongs to

the Latin American Lidar Network (http://lalinet.org), a federative coordinated lidar network focused on the vertically-resolved monitoring of the particle optical properties distribution over Latin America (Guerrero-Rascado et al., 2014; Guerrero-Rascado et al., 2016). The MSP-Lidar I system comprises a commercial Nd:YAG laser operating at 355 nm and 532 nm. The output energy per pulse is 400 mJ for 532 nm and 230 mJ for 355 nm, at a repetition rate of 10 Hz and pulse duration of 5 ns. Elastic backscatter lidar profiles at 532 nm data and air mass modelling trajectories were used in order to evaluate the relationship that trace-element variability have with sea-salt transport and biomass burning apportionment. The lidar backscatter profiles can provide information about the vertical distribution of aerosol layers. By combining those data with the air mass trajectories, it is possible to infer the local sources and transport times for the aerosol plumes to arrive at the SPMA. The retrieval of the aerosol optical properties is based on the measurements of the light backscattered by aerosols, which allows us to obtain the aerosol backscatter coefficient ($\boldsymbol{\beta_a}(\boldsymbol{\lambda,z})$, where β_{aer} is the aerosol backscatter and z is the altitude) at 532 nm. The determination of the vertical profile of the aerosol backscatter and extinction coefficients ($\boldsymbol{\alpha_a}(\boldsymbol{\lambda,z})$) relies on the lidar inversion technique following the Klett-Fernald-Sasano algorithm (Klett, 1981; 1983; Fernald, 1984, Sasano and Nakane, 1984) under the assumption of the single scattering approximation. To solve the lidar equation requires establishing a relationship between $\boldsymbol{\alpha_a}(\boldsymbol{\lambda,z})$ and $\boldsymbol{\beta_{aer}}(\boldsymbol{\lambda,z})$. This is typically achieved by assuming that the aerosol extinction-to-backscatter ratio is independent of altitude that $(\boldsymbol{\lambda})=\boldsymbol{\alpha_{aer}}(\boldsymbol{\lambda,z})/\boldsymbol{\beta_{aer}}(\boldsymbol{\lambda,z})$. To derive the appropriate values of the vertical profile of aerosol backscatter coefficient in the lower troposphere, we use an iterative inversion approach that tunes the LR values based on the inter-comparison of the aerosol optical depth (AOD) (Marenco et al., 2002) values derived from the lidar and collocated AERONET - Aerosol Robotic Network sunphotometer data (Holben et al., 1998) or in some cases from Aqua and Terra Satellite Moderate Resolution Imaging Spectroradiometer (MODIS) data (Remer et al., 2005).

Air masses trajectories are computed using the Global Data Assimilation System (GDAS), an operational system from the National Weather Service National Centers for Environmental Prediction. The GDAS is used as an input in the HYSPLIT model (version 4.8). Forward or backward trajectories are selected on a case-by-case basis, and the model vertical velocity option is chosen (Draxler and Hess, 1998). These trajectories provide the source of air masses arriving at the MASP at different levels (altitudes) and preset time intervals, the coordinates of the IAG, where the instruments are installed, constituting a starting point.

3 Results and discussion

3.1 Meteorological parameters, CCN and PNC

This study was conducted in the winter, when the climate is mostly dry, although three rain events were observed during the study period. Meteorological parameters, PNC and CCN counts are presented in Table 1. As can be seen, the mean temperature was highest on day 5, whereas it was lowest on days 7 and 8, the greatest variation in temperature (16.1°C) occurring on day 11. The mean relative humidity (RH) was above 70% on all days except days 4 and 5, when it was 62%

and 58%, respectively. The greatest variation in RH occurred on days 3, 4 and 11. Precipitation events were observed in the morning, on day 6, and at night, on days 11 and 13 (Fig. 2a). Figure 2 shows hourly variations in meteorological variables (temperature, RH and precipitation), CCN and PNC. The PNCs were highest between 0700 h and 1900 h, whereas they were lowest between 1900 h and 0700 h (Fig. 2b), hereafter referred to as the daytime and nighttime periods, respectively. During the daytime period, PNCs were elevated, especially during the rush hours, primarily associated with vehicular emissions. However, CCN peaks showed the opposite behaviour, CCN concentrations being higher during the afternoon and the nighttime period. These patterns are discussed further in section 3.4. As expected, periods of precipitation were characterised by lower PNCs and CCN concentrations. To eliminate possible interference with the data analysis, we excluded CCN and PNC values for the periods of precipitation. The diameter peaked at less than 100 nm and presented a mean value of approximately 55 nm for all days. The mean peak diameter was highest (92 nm) on day 6 and lowest (29 nm) on day 14, characterising Aitken mode (25-100 nm) (Dal Maso et al., 2005). The mean PND was 44 nm and 62 nm for the daytime and for nighttime periods, respectively, the difference being attributed to the high PNCs during the morning hours. The particle size distributions and NPF events are discussed in section 3.2.

To compare our PNC and CCN values with those of other studies, we plotted our results against the results of recent studies conducted in other urban regions (Fig. 3, Table S1 on Supplementary Information). The PNCs were higher during the daytime period than during the nighttime period, whereas, CCN concentrations were comparable between the two periods. The higher PNCs during the daytime period were expected, given the increased emission of pollutants from local sources such as vehicular traffic. However, the fact that CCN concentrations did not vary significantly between the nighttime and daytime periods indicates that CCN formation was more efficient during the nighttime period. In a study conducted in Beijing, Gunthe et al. (2011) reported similar behaviour for fresh pollutant emissions and regional aged pollution, the latter presenting higher efficiency for CCN formation, as evidenced by lower PNCs and higher CCN concentrations. Those observations are supported by Köhler theory predictions, related to the greater efficiency of larger particles in CCN formation, which is extensively discussed in section 3.4.

The overall mean PNC and CCN values obtained in the present study were similar to those observed by Almeida et al. (2014) for the MASP during October 2012. However, our PNC values were lower than those reported for the MASP by Backman et al. (2012) for October 2010 and January 2011. This variability can be attributed to different meteorological conditions, seasonal differences and the decrease in SO_2 emissions associated with the recently mandated reduction in sulphur concentrations in diesel fuel (Kumar et al., 2016; CETESB, 2015). In a study conducted in Shanghai, Leng et al. (2013) reported PNC values similar to those obtained for the SPMA in the present study, although the CCN concentrations reported by those authors were higher; that might be related to the coastal environment, which increases the concentrations of most soluble compounds, such as ionic species (SO_4^{-2}, NO_3^-, Na^+, Cl^-, K^+), in the aerosol chemical composition. Our results showed PNC values similar to those observed for London and Madrid (Reche et al., 2011; Gómez-Moreno et al., 2011, respectively). In these three urban areas (London, Madrid and the MASP), transport emissions constitute the main pollution source and there are light industries around urban regions. London and Madrid have higher population densities

than does the MASP. However, the vehicle fleet in the MASP is larger than is that in any of the other urban regions evaluated, although Madrid has the highest vehicle/inhabitant ratio and the highest proportion of diesel-powered vehicles (~50%). With a population of over 20 million, Mexico City is the largest megacity in North America. Although comparable to the MASP, the mean PNC for Mexico City in 2006 was double that reported for the 2012–2014 period in the MASP

5 (Kalafut-Pettibone et al., 2011; Almeida et al., 2014; This study). Nevertheless, the mean PNC reported for Mexico City was similar to that observed for 2010 in the MASP (Backman et al., 2010). As previously mentioned, the lower PNCs in the MASP can be attributed to legislation that mandated a reduction in the concentration of sulphur in diesel fuel. The CETESB reported a ~10% reduction in the emission of particulate matter from diesel-powered vehicles between 2010 and 2015. In the MASP, such vehicles emitted 26% of all particulate matter attributed to anthropogenic sources during 2015 (CETESB 2016).

10 In the case of Mexico City, 50% of all particulate emissions in 2006 were from diesel-powered vehicles (Kalafut-Pettibone et al., 2011).

3.2 Daytime PND variability and NPF events

Figure 4a shows the variability in UV radiation intensity, as well as in the concentrations of SO_2, O_3, NO and NO_x. The

15 gaseous concentrations measured at the four CETESB stations were selected according to the direction of the prevailing winds. For the most part, the daytime periods presented high UV intensity (~30 W m^{-2}) and O_3 concentrations (80–100 µg m^{-3}). On days 4, 5, 6, 12 and 14, NO and NO_x concentrations were elevated (100–420 ppb), which was mainly associated with vehicular emissions and prevailing winds from the north-west and north-east. The Marginal Pinheiros and Marginal Tietê roadways are approximately 1 km and 4 km, respectively, from the sampling site. In 2014, approximately 80% of total

20 NO_x emissions in the MASP were attributed to vehicular traffic (CETESB, 2015). Figure 4a also shows that the higher O_3 concentrations were preceded by NO_x peaks. This pattern was expected, given the chemical reactions that occur between NO_x and VOCs in the presence of UV radiation, which induces photochemical activity and the formation of secondary pollutants such as O_3 and SOAs (Monks et al., 2015).

Sulphate and nitrate compounds, which are formed by SO_2 and NO_x precursors, are important components of the nucleation

25 process. The SO_2 concentrations measured at CETESB stations were plotted according to wind direction in order to represent air masses arriving at the measurement site (Fig. 4a). The highest concentrations of SO_2 were associated with winds from the south-east (Congonhas station), whereas winds from north were associated with lower SO_2 concentrations. To the south-east, there are two large industrial areas that represent an important source of SO_2 (Fig. 1). During 2014, industrial activities accounted for 56.9% of the sulphur oxides emitted in the MASP. The SO_2 transport from industrial areas is supported by

30 some studies, which showed that marine air masses and industrial emissions from Cubatão reached the MASP. Sea-salt transport is discussed further in section 3.3, based on the PMF and trajectory analyses.

In order to identify NPF events, we adopted the following requirements described by Dal Maso et al. (2005), which have been extensively employed in other studies (Backman et al., 2012; Betha et al., 2013; Ma and Birmili, 2015): a distinctly

new particle mode (nucleation mode, particle diameters <25 nm) must appear in the size distribution; and the new mode must present a duration of several hours and show growth over time. These requirements were complemented by Ma and Birmili (2015), who stated the following: a sudden increase in PNC, above nighttime background concentration, must occur in nucleation mode; the burst must be sustained for a minimum of 1 h; and a decrease in the concentration of the nucleation mode particles is expected at end of day.

Dal Maso et al.(2005) identified two classes of NPF events, the first of which is divided into two subclasses: (Ia) a clear and pronounced particle formation event, followed by particle growth; (Ib) a particle formation event in which particle growth can be observed from the nucleation, although without a clear nucleation burst; and (II) a particle formation event in which particle growth from nucleation mode cannot be determined.

The contour of the PNDs was plotted in order to identify and classify NPF event days (Fig. 4c). An NPF event meeting all of the requirements described above was observed on day 12. The nucleation burst presented a duration of 3h, followed by particle growth until the beginning of the nighttime period, when a brief decrease in the concentration was observed. An NPF event occurring on day 14 was classified as class II because there was no significant particle growth after nucleation. That event presented nucleation bursts similar to those observed in Singapore by Betha et al. (2013) and in Brisbane, Australia, by Cheung et al. (2011). Those authors associated the events with winds from industrial areas, which carried large quantities of SO_2 and VOCs. There were also NPF events on days 7, 8 and 10, all of those events being categorised as class Ib, clearly showing particle growth throughout the daytime period. On those days, moderate to high concentrations of SO_2 (5–20 µg m^{-3}) were observed at the Congonhas station, which suggests that the nucleation process began near that station, followed by the detection of particle growth at the USP station. Backman et al. (2012) observed similar class Ib events in the MASP.

The nucleation of primary aerosol occurs near local sources such as vehicular and industrial emissions. No nucleation events of that type were detected in the present study because of the distance between the sources and measurement site. However, five different secondary aerosol NPF events were identified. The class Ia and II events were mostly associated with high concentrations of NO_x and O_3, as well as with photochemical activity, whereas the class Ib events were characterised as NPF passing through the measurement site only after the initiation of the event. The impact that those NPF events have on the AR (Fig. 4d) and on D_{act} are discussed in section 3.4.

As previously mentioned, O_3 plays a fundamental role in SOA formation via VOC oxidation, its concentrations being indicative of the efficiency of the photochemical process (Sorribas et al., 2015). However, after the nucleation process, SOAs drive particle growth to larger sizes, primarily by condensation of non-volatile molecules (Pierce et al., 2012; Donahue et al., 2013). In addition, the particle growth rate is the most important factor in determining the extent to which new particles become CCN during NPF events (Leng et al., 2013). As can be seen in Figs. 4a and c, the NPF events observed on days 7 and 8 occurred at low O_3 concentrations, whereas those observed on days 10, 12 and 14 occurred at high O_3 concentrations. To assess the importance of photochemical activity and SOA production to particle diameter and to the AR, we plotted NPF events under low and high O_3 concentrations (Fig. S1, on Supplementary Information). As expected, particles formed during

low-O_3 NPF were smaller than were those formed during high-O_3 NPF (Fig. 4c). In addition, the AR was higher for the particles formed during high-O_3 NPF than for those formed during low-O_3 NPF. That is in agreement with the findings of studies predicting or demonstrating the efficiency of SOA condensation in inducing particles to become CCN (Pierce et al., 2012; Riipinen et al., 2011)

5   We drew PND contour plots in order to evaluate particle nucleation and growth progression during NPF events of the various classes and even on non-NPF event days. The proportional distribution of hourly PNCs in three modes (nucleation, Aitken and accumulation (100-1000 nm))was also plotted, as were the hourly PNDs (Fig. 5). The NPF event on day 12 showed a nucleation burst between 1000 h and 1500 h (Fig. 5a), which was confirmed by the fact that the proportion of particles in nucleation mode was higher (>50%) during that period than at any other time on that day. The particle growth in

10   subsequent hours was accompanied by an increase in the proportion of particles in Aitken mode, as can be noted in the hourly PNCs and PND (Fig. 5a).

The class Ib NPF events showed characteristic particle growth after midday, with probable occurrence of a nucleation event, which was not observed between 1000 h and 1200 h. That particle growth was also detected by a higher PNC (63%) of Aitken mode at 1500 h and an increase in peak diameters between 1200 h and 1500 h (Fig. 4b). It is noteworthy that the

15   proportion of particles in Aitken was high (>45%) for most hours on the three selected days, which indicates a continuous increase in the size of primary and new particles. This observation is supported by the fact that the local traffic presents constant emissions, with high density during the daytime period and low density during the nighttime period, which agrees with the total PNC values shown in the hourly frequency graphics (Fig. 5).

3.3 Apportionment of vehicular traffic, biomass burning and sea salt from remote sources

20   A combination of lidar, HYSPLIT trajectory, size-distributed chemical composition and PMF analysis (Na, Ni, Cr, Ca, Ti, K, Cl P, Fe, Mn, Pb, Cu, Zn, S and BC) analyses were used in order to apportion the contribution of sea-salt and biomass burning within the air masses arriving at the MASP. Over the past 30 years, various studies conducted in the MASP have employed receptor modelling and aerosol chemical composition analysis in order to identify the main sources of atmospheric pollutants (Bouéres and Orsini, 1981; Andrade et al., 1994; Castanho and Artaxo, 2001; Sanchez-Ccoyllo and Andrade,

25   2002; Sanchez-Ccoyllo et al., 2008; Andrade et al., 2012). Those studies have determined that vehicular traffic account for 50–60% of fine particles, thus constituting the main source, followed by oil boilers (accounting for 20–40%), road dust (accounting for 10–30%), industrial emissions (accounting for 10–20%), biomass burning (accounting for 10–20%) and construction activities (accounting for ~10%). Some studies carried on in the MASP evaluated the elemental profiles of the principal urban pollution sources, characterising observed elements such as Mn, Pt, Ni, Cu, Cr and Zn as markers of gasoline

30   and alcohol emissions (Silva et al.,2010). Diesel burning by heavy-duty vehicles is associated mainly with BC and S. Suspended road dust, characterised inside and outside road tunnels, has been found to be comprise BC, Si, Al, Fe, Ca, Mg, K, Ti and S, which denotes a mixture of soil, pavement abrasion, tire wear, brake wear and vehicular emission (Hetem and Andrade 2016). In a general approach, other studies found BC to be related to biomass burning; Na and Cl to be related to

sea-salt contribution; and Fe, Cu, Zn, Cr, Pb and Ni to be related to industrial emissions (Bzdek et al., 2012; Calvo et al., 2013; Taiwo et al., 2014).

Figure 6 shows the mass size distributions of trace elements from MOUDI membrane samples for different periods. The concentrations of BC were high (~0.9%) on days 6, 12 and 13 (Fig. 6a), whereas they were intermediate (~0.4%) on days 7, 8, 9 and 14. The concentrations of Cl, K and Pb were high on days 8 and 9 (Fig. 6b–d), and the concentration of K was intermediate (~0.2 µg cm^{-3}) on day 6. The elements Ti, Cr, Ca and Cu showed intermediate concentrations for most days, with peaks on days 6 and 12 (Fig. 6e–h). In order to assess the source apportionment of aerosol mass concentration, a PMF analysis was applied to trace-element, BC and carbon monoxide (CO) concentrations. The CO is an important marker associated with vehicular emissions in urban areas, its concentrations being measured at the Marginal Tietê. Our analysis showed that vehicular traffic had a great influence on all days, mainly during the daytime, and vehicular emissions + biomass burning had an influence only on days 6, 12 and 13, whereas sea-salt + industrial emissions had an influence only on days 7 and 8 (Figure S4 in the Supplementary Information).

Various studies have identified vehicular traffic as the main local pollutant source in MASP. The contribution of vehicular traffic is higher during the daytime and lowerduring the nighttime. Some species, such as Cr, Ti, Cu and BC, are frequently used as markers for vehicular traffic (Andrade et al., 2012). In this study, those compounds showed a strong correlation with CO during daytime. We also observed that BC and Cu correlated strongly with CO during nighttime, as illustrated in Figure S5 (Supplementary Information). In addition, the strong correlation between vehicular traffic marker species and CO confirms that vehicular traffic was the predominant daytime source on all days. The strong correlation of BC and Cu with CO at nighttime can be related to vehicular emission + biomass-burning events, as demonstrated by the PMF analysis.

Figures 7c and 7d present the vertical profile for two measurement days obtained with the MSP-Lidar I system. On day 6, several thin aerosol plumes were detected above the planetary boundary layer (PBL). According to the range-corrected lidar signal (Fig.7c), most of the aerosol load in the atmosphere is concentrated inside the PBL, approximately 500 m above ground level (AGL). However, several aerosol layers can clearly be seen above the PBL, at 1000–2000 m AGL, and a thin aerosol layer can be seen at approximately 3000 m AGL. The mean aerosol backscatter profile at 532 nm (Fig.7c), retrieved applying the Klett inversion method, as previously described, showed a peak of 0.006 km^{-1}sr^{-1}at approximately 500 m AGL, representing all aerosol trapped inside the PBL, and another peak of 0.0018 km^{-1}sr^{-1} at approximately 2800 m AGL. The mean aerosol vertical profile at 532 nm clearly shows a backscatter signal from aerosol plumes up to 4000 m AGL, which would typically be from a source outside the MASP.

When the lidar data were analysed by tuning the LR values based on the inter-comparison of the MODIS-derived AOD, a mean lidar ratio of 70±14 sr was obtained, which is within the range associated with absorbing particles from biomass burning (Müller et al., 2007; Baars et al., 2015). The air mass backward trajectories simulated using the HYSPLIT model (Fig. 7a) strengthens the hypothesis that aerosol from biomass burning was transported from the northern and central-west portion of Brazil, where there were several fire focus, reaching higher levels and being transported to the MASP at altitudes of 3000–4000 m AGL. The same pattern was found for day 12 (Fig. 7d) and 13 (Fig. S6, in the Supplementary Information),

when thin aerosol plumes were also detected above the PBL, at 2400–4000 m AGL, as can be seen in the mean backscatter profile (Fig. 7d). The mean lidar ratio for this case was also 70±14 sr, again associating the plumes with a biomass-burning aerosol type. Air masses trajectories (Fig.7b) indicated that plumes detected at the MASP by the lidar system had been transported from the central-west portion of the country and had travelled across regions with several fire focus. The lidar

5   data analyses were in agreement with the PMF analysis and size distribution of elemental concentrations in samples collected by MOUDI on days 6, 12 and 13, when high concentrations of BC were observed. In addition, the higher variability of Cu, Cr, Ni and CO concentrations on those days, obtained in the PMF analysis, indicates an association between biomass burning and vehicular emissions.

Previous studies have shown the contribution of sea salt to the aerosol profile in the MASP (Andrade et al., 1994; Castanho

10   and Artaxo, 2001; Vara-Vela et al., 2016). As can be seen in Fig. 4b, the prevailing wind direction was from the south-east during the nighttime period on days 7 and 8, which is in line with the low-altitude air mass trajectories shown in Fig. S2 in the Supplementary Information; the higher concentrations of Na and Cl indicate sea-salt transport from the coastal region, as evidenced by the increased Pb concentrations on those days. Normally, Pb is linked to emissions from anthropogenic sources, mainly industrial emissions, as the contribution from fuel burning has decreased substantially after the ban on Pb in

15   gasoline fuels. Using Pb isotopic signatures, Gioia et al. (2010) demonstrated by aerosols from the Cubatão industrial area arrive at the MASP when south-east wind predominates. As can be seen in Fig. 1, Cubatão is located in the coastal region, corroborating the sea-salt transport. Figure 8c shows the range-corrected signal of the MASPMSP-Lidar I system in the atmosphere throughout day 4. Between 2030h UTC and 2213h UTC, signal attenuation was detected at 500–1000 m AGL, which is associated with the intrusion of clean air at the PBL of the MASP. Typically, such intrusion is related to sea breeze

20   transported to MASP (Rodrigues et al., 2013). The mean backscatter profile showed the presence of aerosol only within the PBL, where a smaller aerosol backscatter signal could be seen between 300 m and 1200 m AGL, associated with the clean air region inside the PBL. The mean lidar ratio for this measurement was 40±8 sr, which is within the range associated with the urban aerosol type (Baars et al., 2015). These observations are corroborated by the PMF analysis, which showssea-salt +industrial emissions contribution for days 7 and 8 associated to Na, Cl, Pb, Fe, Zn and S.

25   In summary, sea-salt air masses arriving at the MASP were observed during the nighttime period on three of the days evaluated. During the nighttime periods of days 4, sea-salt events were observed by lidar, whereas they were identified by the PMF analysis using trace-element concentration during the nighttime period of days 7 and 8. Throughout the year, sea breezes arrive at the MASP in the afternoon and evening (Oliveira et al., 2002; Freitas et al., 2007). In the present study, plumes generated from biomass burning were detected by lidar and PMF analysis on days 6 and 12 and 13, being associated

30   to vehicular traffic with an increase in BC and CO on those specific days. In Brazil, numerous biomass-burning events occur every year from July to November, mainly in the central and northern regions of the country. However, many such events, associated with agricultural activities, occur within the state of São Paulo throughout the year (Kumar et al., 2016). All focus fire, as shown in figures 7a and 7b, were identified from Geostationary Operational Environmental Satellite images. In addition, vehicular traffic predominance during daytime could be observed, in line with several source apportionment studies

carried out in MASP.

3.4 Effects of vehicular traffic, remote sources and NPF events on CCN activation properties

The mean AR values were 0.22±0.05 (at 0.2%), 0.33±0.09 (at 0.4%), 0.41±0.05 (at 0.6%), 0.48±0.09 (at 0.8%) and 0.53±0.09 (at 1.0%), being nighttime means twice as high as the daytime means for all supersaturation levels (Table 2 and Fig. 9a). In addition, the PNC was five times higher during daytime than nighttime. Vehicular traffic was identified as the main daytime local pollutant source on all days. In order to determine the effects that NPF events have on ARs, the mean values were split into daytime (with vehicular traffic) and nighttime periods with and without NPF or remote source events (non-event), as seen in Fig. 9a. We observed a tendency for ARs to be lower during daytime with NPF than those without, although we observed no such tendency for nighttime periods. That is in agreement with the findings of previous studies suggesting that larger particles act more efficiently as CCN than do smaller particles (Sihto et al., 2011; Dusek et al., 2010). In a study conducted in Finland, some events featured NPF bursts, followed by particle growth. During those events, the ARs were very low, due to higher PNCs and smaller particle sizes (Sihto et al., 2011). In the present study, the AR increased substantially after each NPF event, although it was still lower than that observed on the non-event days. In addition, we observed increase in the number of CCN during the nighttime periods after NPF events, as showed in Supplementary Information (Fig. S3), attributed to the high rate of growth among the particles formed during NPF, an observation that is supported by previous studies (Sihto et al., 2011; Yue et al., 2011; Peng et al., 2014).

Figures 4c and 9 show the predominance of larger particles during the nighttime, as a result of primary and secondary aerosol growth during the daytime period. Therefore, the higher AR during nighttime was an expected finding, given the efficiency of larger particles to act as CCN. During the daytime vehicular traffic, the mean AR values were similar to those observed in other urban areas, although not to those observed in coastal areas (Leng et al., 2013; Furutani et al., 2008), as indicated by recent studies of fresh urban pollution conducted in the MASP, Vienna and Beijing (Almeida et al., 2014; Burkartet al., 2012; Gunthe et al., 2011). However, the AR reported for Beijing was twice that found for the MASP in the present study, considering entire campaign for both, although the PNC values were similar. In addition, the AR values observed for the SPMA in the present study are comparable to the fresh ship exhaust emissions reported in a study conducted along the coast of California (Furutani et al., 2008). The nighttime AR values observed for the MASP were similar to those reported in a study conducted in a forest environment (Sihto et al., 2011) and in the coastal environments, although opposite those observed in others urban environments (Table 2). However, the mean nighttime AR and PNC values were higher for aged pollution in Beijing than for the MASP.

Figure 9b shows the hourly mean AR values fordays with and without NPF. The AR values were lowest between 1000 h and 1500 h, whereas they were highest during the nighttime period. The AR began to decrease after 0600 h and subsequently began to increase after 1500 h. In the MASP, the morning rush occurs between 0700 h and 1000h, whereas the afternoon rush occurs between 1700 h to 2000 h. The decrease begin and the lower values of AR occurred during the morning rush and

formation of a secondary aerosol. Vehicular traffic and secondary aerosol formation constitute the main sources of particles in megacities such as the MASP (Andrade et al., 2012 and prior studies). As previously discussed, the formation of secondary aerosols is favoured by photochemical reactions, which depend on solar radiation (UV and visible wavelength light), O_3 and hydroxyl radicals. Figure 4a shows UV radiation and O_3 peak at midday, after which there is secondary aerosol

5   formation and growth as demonstrated by intermediate and high concentrations in nucleation and Aitken modes, respectively, in the afternoon (Fig. 4c).

The variability in NO_x and CO concentrations measured at the Marginal Tietê is mainly associated with vehicular traffic, because fuel combustion is the predominant source of such pollutants in the MASP. As can be seen in Fig. 9b and Fig. 10c, an increase in NO_x occurred during the morning rush and was clearly related to the decrease in AR and particle diameter

10   mode (Fig. 9b), as well as to the increase in D_{act} (Fig. 10c). The NO_x decrease after midday was not associated with the decrease in traffic volume but with photochemical reactions and secondary formation of pollutants, as previously discussed. We believe that the NO_x and O_3 variability corroborates our assumption, explaining the decrease in AR values during the daytime period in the presence of high vehicular traffic volume and secondary aerosol formation.

The increase in AR after 1500 h can be correlated with the increase in particle diameter and CCN concentrations. In addition,

15   the production of SOAs by VOC degradation can result in the formation of polar functional groups that contribute to the growth and hydrophilicity of particles. Therefore, aged aerosols emitted and formed during the morning from vehicular traffic and secondary particles mainly showed an increase in AR at the end of the afternoon and during the nighttime period. This observation is in agreement with those of previous studies in which increased CCN activation was associated with aged anthropogenic emissions (Quinn et al., 2008; Furutani et al., 2008; Dusek et al., 2010; Bougiatioti et al., 2011; Zhang et al.,

20   2014). Nevertheless, vehicular emissions from afternoon rush (1700–2000 h) had less effect on the AR than did those from the morning rush, probably due to the absence of secondary aerosols and mixing with aged aerosols. The hourly particle diameter mode clearly shows the effect of particle size on AR values, lower ARs being accompanied by smaller particle size modes (Fig. 9b). Our observation is in agreement with those of previous studies demonstrating the strong effect of particle size on CCN activity.

25   The overall mean D_{act} varied between 54 nm (at SS = 1.0%) and 155 nm (at SS= 0.2%) for the nighttime and daytime periods, respectively. A comparison between the D_{act} values obtained in this study and those reported in the literature is shown in Table S2. As can be seen in Fig. 10a, D_{act} presents non-linear decrease as function of increase in supersaturation. The D_{act} was higher during the daytime period than during the nighttime period, as was expected given the AR data. The mean D_{act} values for daytime with vehicular traffic + biomass burning and vehicular traffic + NPF events were similar to

30   those observed for those days with vehicular traffic only. The D_{act} values for nighttime after NPF or during sea-salt + industrial emissions events were similar to those observed after non-event days, although the D_{act} values were slightly higher for nighttime during which there were biomass-burning plumes + vehicular traffic, mainly when the SS < 0.6%. At high supersaturation values, particles with different chemical composition and therefore hygroscopicity have only a weak effect on CCN activity (Sihto et al., 2011; Zhang et al., 2014).

Figure 10c shows the time series of the mean D_{act} values for days with and without NPF events. The D_{act} values recorded during rush hours were higher on days with NPF than on those without. A number of hours before the occurrence of NPF events in which lower PNCs and larger particles predominated (Fig. 4c and Fig. 10c), lower AR values and higher D_{act} values were observed (Fig. 9b and Fig. 10c, respectively). This observation could be related to a possible increase in SOA precursor

5 compounds in condensed phases before NPF events. Some of those compounds are monoterpenes and aromatic compounds, which have been reported to present low hygroscopicity (Kroll and Seinfeld, 2008). Except during the above mentioned pre-NPF periods, days with and without NPF events showed similar nighttime means.

The efficiency of aerosol particles to act as CCN can be estimated on the basis of AR and D_{act} data. The AR is dependent on particle size and chemical composition, whereas D_{act} is dependent on chemical composition only (Furutani et al., 2008). As

10 can be seen in Fig. 10b, the non-linear correlation between AR and D_{act} can be related to different chemical composition and size distribution of aerosol. During daytime, the D_{act} was increased and the AR was decreased, whereas the inverse was true for the nighttime. In general, the daytime period is associated with particles that are less hygroscopic and smaller, mainly emitted by vehicular traffic and formed in NPF events. However, the decreased D_{act} and increased AR were observed in the nighttime period, being associated with larger and more hygroscopic particles. Our observations support the assumption that

15 nighttime samples typically comprise greater concentrations of water soluble species, such as $(NH_4)_2SO_4$, SOA, NO_3^-, and of marine air than do daytime samples. Our findings are also in keeping with those of other studies showing that aged aerosols present high hygroscopicity (Gunthe et al., 2011; Bougiatioti et al., 2011).

We compared the D_{act} values obtained in this study with those reported in previous studies (Fig. 11 and Table S2). Our nighttime (non-event) means were similar to those reported for continental air masses over Shanghai (Leng et al., 2013), for

20 the atmosphere over a boreal forest in Finland (Sihto et al., 2011) and for periods without air masses containing anthropogenic emissions over California (Furutani et al., 2008), as detailed in Table S2, on Supplementary Information. The mean D_{act} values for non-event nighttime periods and during sea-salt events were comparable to those observed for the Atlantic and Pacific Oceans, as well as for the Gulf of Mexico and for aged anthropogenic emissions in California (Furutani et al., 2008; Quinn et al., 2008). Our daytime with vehicular traffic means were comparable to those reported for

25 urban/industrial and fresh polluted air masses in Mexico and California (Quinn et al., 2008), even the differences being less than statistically significant (Fig.11).

As can be seen in Figure 12b, days with vehicular traffic + NPF showed lower AR values than did those with vehicular traffic + biomass burning and those with vehicular traffic only, without daytime events. In addition, AR values were slightly different at nighttime. The nighttime increase in AR after NPF events was related to particle growth (Fig. 12b). In relation to

30 D_{act}, during nighttime, biomass-burning events promoted slightly higher D_{act} values than did NPF and sea-salt transport, which is attributable to lower particle hygroscopicity. Although there was a lack of statistical significance, we observed a tendency for biomass burning to affect the air masses arriving at the MASP by decreasing the activation properties.

4 Summary and conclusions

The activation of CCN is quite important to cloud formation and consequently to the hydrological cycle. The aim of this study was to evaluate the variability in CCN activation parameters under the influence of local sources, remote sources, and NPF, in order to assess the impact of those events on CCN activity in the MASP. The regional atmosphere is highly affected by vehicular traffic emissions, and lower by remote sources such as biomass burning and sea-salt transport.

During daytime, PNCs were higher and particle sizes were smaller than during the nighttime periods, a finding that was attributed to fresh vehicular emissions and NPF, whereas the lower PNCs and larger particle sizes observed during the nighttime periods were attributed to the ageing and post-growth deposition of particles (Fig. 12a). Five NPF events were identified, four being of the class I type. In addition, NPF events were found to have a significant effect on particle size distribution. Biomass-burning and sea-salt air masses were identified by a combination of lidar analysis, HYSPLIT trajectory and PMF analysis and size-distributed chemical composition.

The AR and D_{act} CCN activation parameters presented a clear pattern for the daytime (vehicular traffic) and nighttime periods, the daytime period featuring higher D_{act} and lower AR. The size distribution made a marked contribution to that pattern, according to the assumption that larger particles are more efficient for CCN activation than are smaller particles. That hypothesis is supported by AR and D_{act} differences between days with and without NPF events. Slight differences for activation parameters could be observed among sea-salt- and biomass-burning-influenced air masses, as well as non-event nighttime periods (Fig. 12c and Fig.12d). Those slight differences can be explained by complex mixtures between aerosols from local and external sources, the latter travelling longer distances before reaching to the measurement site. Dilution, mixing and ageing of aerosols from remote sources occur during travel from the source emission area to the measurement site. The D_{act} calculated for sea-salt air masses in this study were comparable to that observed over the Atlantic and Pacific Oceans. In summary, our results showed that vehicular traffic during the daytime had greater negative effects on activation parameters than did remote sources or vehicular traffic at nighttime. However this evidence must be confirmed by long-term measurements in future studies.

This was the first study to evaluate the effects of vehicular traffic, remote sources and NPF events on CCN activation properties in urban area on South America and only the second to assess CCN variability in the MASP. Our results show the influence that vehicular traffic, long-range transport of sea-salt, biomass-burning plumes and NPF events have on CCN properties. Therefore, long-term studies covering different seasons and sampling site environments (e.g. coastal, urban and rural) are needed in order to represent CCN variability more accurately under diverse environmental conditions. To improve understanding of the influence that aerosol composition and provenance have on CCN activity, real-time monitoring of aerosol chemical composition and CCN size distribution is also necessary.

Acknowledgements

This work received financial support as part of the University Global Partnership Network (UGPN)for the "Emissions and

role of fine aerosol particles in the formation of clouds and precipitation (eRAIN)"project grant, awarded jointly to Universities of Surrey and São Paulo. This study is also part of a major project entitled "Narrowing the Uncertainties in Aerosol and Climate changes in the state of São Paulo (NUANCE)", funded by the *Fundação de Amparo à Pesquisa do Estado de São Paulo* (FAPESP, São Paulo Research Foundation). Carlos Eduardo Souto-Oliveira is the recipient of a PhD scholarship from the Brazilian *Coordenação de Aperfeiçoamento de Pessoal de Nível Superior* (CAPES, Office for the Advancement of Higher Education).

References

Almeida, G.P., Brito, J., Morales, C.A., Andrade, M.F., and Artaxo, P.: Measured and modelled Cloud Condensation Nuclei (CCN) concentration in São Paulo, Brazil: the importance of aerosol size-resolved chemical composition on CCN concentration prediction, Atmos. Chem. Phys., 13, 1–36, doi:10.5194/acp-14-7559, 2014.

An, J., Wang, H., Shen, L., Zhu, B., Zou, J., Gao, J., and Kang, H.: Characteristics of new particle formation events in Nanjing, China: Effect of water-soluble ions, Atmos. Environ., 108, 32–40, doi:10.1016/j.atmosenv.2015.01.038, 2015.

Andrade, M.F., De Miranda, R. M., Fornaro, A., Kerr, A., Oyama, B., De Andre, P. A., and Saldiva, P.: Vehicle emissions and PM 2.5 mass concentrations in six Brazilian cities, Air Qual., Atmos. Health, 5, 79–88, doi: 10.1007/s11869-010-0104-5, 2012.

Andrade, M.F., Orsini, C., and Maenhaut, W.: Relation between aerosol sources and meteorological parameters for inhalable atmospheric particles in Sao Paulo City, Brazil, Atmos. Environ., 28, 2307–2315, doi:10.1016/1352-2310(94)90484-7, 1994.

Andreae, M. O.: The aerosol nucleation puzzle, *Science*, *339*, 911–912, doi:10.1126/science.1233798, 2013.

Andreae, M. O., and Rosenfeld, D.: Aerosol–cloud–precipitation interactions. Part 1. The nature and sources of cloud-active aerosols, Earth-Sci. Rev., 89, 13–41, doi:10.1016/j.earscirev.2008.03.001, 2008.

Andreae, M. O., Rosenfeld, D., Artaxo, P., Costa, A.A., Frank, G. P., Longo, K. M., and Silva-Dias, M. A. F.: Smoking rain clouds over the Amazon, Science, 303, 1337–1342, doi:10.1016/j.earscirev.2008.03.001, 2004.

Baars, H., Kanitz, T., Engelmann, R., Althausen, D., Heese, B., Komppula, M., Preißler, J., Tesche, M., Ansmann, A., Wandinger, U., Lim, J.-H., Ahn, J. Y., Stachlewska, I. S., Amiridis, V., Marinou, E., Seifert, P., Hofer, J., Skupin, A., Schneider, F., Bohlmann, S., Foth, A., Bley, S., Pfüller, A., Giannakaki, E., Lihavainen, H., Viisanen, Y., Hooda, R. K., Pereira, S., Bortoli, D., Wagner, F., Mattis, I., Janicka, L., Markowicz, K. M., Achtert, P., Artaxo, P., Pauliquevis, T., Souza, R. A. F., Sharma, V. P., van Zyl, P. G., Beukes, J. P., Sun, J. Y., Rohwer, E. G., Deng, R., Mamouri, R. E., and Zamorano, F.: PollyNET: a global network of automated Raman-polarization lidars for continuous aerosol profiling, Atmos. Chem. Phys. Discuss., 15, 27943–28004, doi: 10.5194/acpd-15-27943-2015, 2015.

Backman, J., Rizzo, L. V., Hakala, J., Nieminen, T., Manninen, H. E., Morais, F., and Kulmala, M.: On the daytime cycle of urban aerosols, black carbon and the occurrence of new particle formation events in springtime São Paulo, Brazil, Atmos. Chem. Phys., 12, 11733–11751, doi: 10.5194/acp-12-11733-2012, 2012.

Betha, R., Spracklen, D. V., and Balasubramanian, R.: Observations of new aerosol particle formation in a tropical urban atmosphere, Atmos. Environ., 71, 340–351, doi: 10.1016/j.atmosenv.2013.01.049, 2013.

Bouéres, L.C.S., and Orsini, C.M.Q.: Fine and coarse elemental components in the urban aerosol of São Paulo, Brazil, Nucl. Instrum. Methods, 181:417–424, doi: 10.1016/0029-554x(81)90643-1, 1981.

5 Bougiatioti, A., Nenes, A., Fountoukis, C., Kalivitis, N., Pandis, S. N., and Mihalopoulos, N.: Size-resolved CCN distributions and activation kinetics of aged continental and marine aerosol, Atmos. Chem. Phys., 11, 8791–8808, doi: 10.5194/acp-11-8791-2011, 2011.

Bucholtz, A.: Rayleigh-scattering calculations for the terrestrial atmosphere, Appl. Optics, 34, 2765-2773, doi:10.1364/AO.34.002765, 1995.

10 Burkart, J., Steiner, G., Reischl, G., and Hitzenberger. R.: Long-term study of cloud condensation nuclei (CCN) activation of the atmospheric aerosol in Vienna, Atmos. Environ., 45, 5751–5759, doi:10.1016/j.atmosenv.2011.07.022, 2011.

Bzdek, B. R., Pennington, M. R., and Johnston, M. V.: Single particle chemical analysis of ambient ultrafine aerosol: A review, J. Aerosol Sci., 52, 109–120, doi:10.1016/j.jaerosci.2012.05.001, 2012.

Calvo, A. I., Alves, C., Castro, A., Pont, V., Vicente, A. M., and Fraile, R.: Research on aerosol sources and chemical 15 composition: Past, current and emerging issues, Atmos. Res., 120–121, 1–28, doi: 10.1016/j.atmosres.2012.09.021, 2013.

Castanho, D. A., and Artaxo, P.: Wintertime and summertime São Paulo aerosol source apportionment study, Atmos. Environ., 35, 4889–4902, doi:10.1016/s1352-2310(01)00357-0, 2001.

Environmental Protection Agency of São Paulo Estate, Air quality report for the State of São Paulo 2014: http://www.cetesb.sp.gov.br/ar/qualidade-do-ar/31- publicacoes-e-relatorios, (in Portuguese), last access: 10 February 2016.

20 Environmental Protection Agency of São Paulo Estate, Air quality report for the State of São Paulo 2015: http://www.cetesb.sp.gov.br/ar/qualidade-do-ar/31- publicacoes-e-relatorios, (in Portuguese), last access: 10 June 2016.

Cheung, H. C., Morawska, L., and Ristovski, Z. D.: Observation of new particle formation in subtropical urban environment, Atmos. Chem. Phys., 11, 3823–3833, doi:10.5194/acp-11-3823-2011, 2011.

Dal Maso, M., Kulmala, M., Riipinen, I., Wagner, R., Hussein, T., Aalto, P. P., and Lehtinen, K. E. J. Formation and growth 25 of fresh atmospheric aerosols: eight years of aerosol size distribution data from SMEAR II, Hyytiala, Finland, Boreal Environ. Res., 10, 323–336, 2005.

Deng, Z. Z., Zhao, C. S., Ma, N., Ran, L., Zhou, G. Q., Lu, D. R., and Zhou, X. J.: An examination of parameterizations for the CCN number concentration based on in situ measurements of aerosol activation properties in the North China Plain, Atmos. Chem. Phys., 13, 6227–6237, doi:10.5194/acp-13-6227-2013, 2013.

30 Donahue, N. M., Ortega, I. K., Chuang, W., Riipinen, I., Riccobono, F., Schobesberger, S., Dommen, J., Baltensperger, U., Kulmala, M., Worsnopbe, D.R., and Vehkamaki, H: How do organic vapors contribute to new-particle formation?, Faraday Discussions, 165, 91. doi:10.1039/c3fd00046j, 2013.

Draxler, R. and Rolph, G: HYSPLIT (Hybrid Single-Particle Lagrangian Integrated Trajectory) Model, NOAA Air Resources Laboratory: http://www.arl.noaa.gov/ready/hysplit4.html, last access: 20 November 2015.

Draxler, R., and Hess G.: Description of the hysplit 4 modeling system, NOAA Tech. Memo. ERL ARL-224, NOAA Air Resources Laboratory: http://ready.arl.noaa.gov/HYSPLIT.php, last access: 2 December 2003.

Dusek, U., Frank, G. P., Curtius, J., Drewnick, F., Schneider, J., Kürten, A., and Pöschl, U.: Enhanced organic mass fraction and decreased hygroscopicity of cloud condensation nuclei (CCN) during new particle formation events, Geophys. Res. Lett., 37, doi:10.1029/2009gl040930, 2010.

Fernald, F.G.: Analysis of atmospheric lidar observations: some comments, Appl. Opt., 23, 652-653, doi:10.1364/AO.23.000652, 1984.

Frank, G.P., Dusek, U., and Andreae, M.O.: A method for measuring size-resolved CCN in the atmosphere, Atmos. Chem. Phys. Discuss., 6, 4879–4895, doi:10.5194/acpd-6-4879-2006, 2006.

Freud, E., Rosenfeld, D., Andreae, M. O., Costa, A. A., and Artaxo, P.: Robust relations between CCN and the vertical evolution of cloud drop size distribution in deep convective clouds, Atmos. Chem. Phys., 8, 1661–1675, doi:10.5194/acp-8-1661-2008, 2008.

Furutani, H., Dall, M., Roberts, G. C., and Prather, K. A.: Assessment of the relative importance of atmospheric aging on CCN activity derived from field observations, Atmos. Environ., 42, 3130–3142, doi:10.1016/j.atmosenv.2007.09.024, 2008.

Gioia, S.M.C.L., Babinski, M., Weiss, D.J., and Kerr, A.A.F.S.: Insights into the dynamics and sources of atmospheric lead and particulate matter in São Paulo, Brazil, from high temporal resolution sampling, Atmos. Res., 98,478–485, doi: 10.1016/j.atmosres.2010.08.016, 2010.

Guerrero-Rascado, J. L., Landulfo, E., Antuña, J. C., Barbosa, H. M. J., Barja, B, Bastidas, A. E., Bedoya, A. E., da Costa, R. F., Estevan, R., Forno, R. N., Gouveia, D. A., Jimenez, C., Larroza, E. G., Lopes, F. J. S., Montilla-Rosero, E., Moreira, G. A., Nakaema, W. M., Nisperuza, D., Alegria, D., Múnera, M., Otero, L., Papandrea, S., Pawelko, E., Quel, E. J., Ristori, P., Rodrigues, P. F., Salvador, J., Sánchez, M. F., and Silva, A.: Towards an instrumental harmonization in the framework of LALINET: dataset of technical specifications in Proc. SPIE 9246, Lidar Technologies, Techniques, and Measurements for Atmospheric Remote Sensing X, 92460O, doi: 10.1117/12.2066873, 2014.

Guerrero-Rascado, J. L., Landulfo, E., Antuña, J. C., Barbosa, H. M. J., Barja, B, Bastidas, A. E., Bedoya, A. E., da Costa, R. F., Estevan, R., Forno, R. N., Gouveia, D. A., Jimenez, C., Larroza, E. G., Lopes, F. J. S., Montilla-Rosero, E., Moreira, G. A., Nakaema, W. M., Nisperuza, D., Alegria, D., Múnera, M., Otero, L., Papandrea, S., Pawelko, E., Quel, E. J., Ristori, P., Rodrigues, P. F., Salvador, J., Sánchez, M. F., and Silva, A.: Latin American Lidar Network (LALINET) for aerossol research: Diagnosis on network instrumentation, J. Atmos. Sol-Terr. Phy., 138–139, 112–120, doi:10.1016/j.jastp.2016.01.001, 2016.

Gunthe, S. S., Rose, D., Su, H., Garland, R. M., Achtert, P., Nowak, A., Wiedensohler, A., Kuwata, M., Takegawa, N., Kondo, Y., Hu, M., Shao, M., Zhu, T., Andreae1, M. O., and Pöschl, U.: Cloud condensation nuclei (CCN) from fresh and aged air pollution in the megacity region of Beijing, Atmos. Chem. Phys., 11, 11023–11039, doi:10.5194/acp-11-11023, 2011.

Hallquist, M., Wenger, J. C., Baltensperger, U., Rudich, Y., Simpson, D., Claeys, M., Dommen, J., Donahue, N. M., George, C., Goldstein, A. H., Hamilton, J. F., Herrmann, H., Hoffmann, T., Iinuma, Y., Jang, M., Jenkin, M. E., Jimenez, J. L.,

Kiendler-Scharr, A., Maenhaut, W., McFiggans, G., Mentel, T.F., Monod, A., Prévôt, A. S. H., Seinfeld, J. H., Surratt, J. D., Szmigielski, R. and Wildt, J.: The formation, properties and impact of secondary organic aerosol: current and emerging issues, Atmos. Chem. Phys., 9, 5155–5236, doi:10.5194/acp-9-5155, 2009.

Heal, M.R., Kumar, P., and Harrison, R.M.: Particles, Air Quality, Policy and Health, Chem. Soc. Reviews, 41, 6606–6630, doi:10.1039/c2cs35076a, 2012.

Hetem, I. G., and Andrade, M. F.: Characterization of fine particulate matter emitted from the resuspension of road and pavement dust in the Metropolitan Area of São Paulo, Brazil, Atmosphere, 7, 31-41, doi:10.3390/atmos7030031, 2016.

Holben, B.N., Eck, T. F., Slutsker, I., Tanré, D., Buis, J. P., Setzer, A., Vermote, E., Reagan, J. A., Kaufman, Y. J., Nakajima, T., Lavenu, T. Jankowiak, I., and Smirnov, A.: Aeronet - A Federal Instrument Network and Data Archive for Aerosol Characterization, Remote Sens. Environ., 66, 1-16, doi:10.1016/S0034-4257 (98)00031-5, 1998.

Holmes, N. S.: A review of particle formation events and growth in the atmosphere in the various environments and discussion of mechanistic implications, Atmos. Environ., 41, 2183–2201, doi: doi.org/10.1016/j.atmosenv.2006.10.058, 2007.

IBGE, Brazilian Institute of Geography and Statistics: http://www.ibge.gov.br/english/, last access: 01 January 2016.

IPCC, Climate change 2013, Scientific basis, Fifth assessment of the Intergovernmental Panel on Climate Change: http://www.ipcc.ch/report/ar5/wg1/, last access: 10 February 2015.

Karavalakis, G., Boutsika V., Stournas S., and Bakeas E.: Biodiesel emissions profile in modern diesel vehicles. Part 2: Effect of biodiesel origin on carbonyl, PAH, nitro-PAH and oxy-PAH emissions, Sci. Total Environ., 409, 938–747, doi:10.1016/j.scitotenv.2010.11.010, 2011.

Klett, J. D.: Lidar calibration and extinction coefficients, Appl. Optics, 22, 514, doi:10.1364/ao.22.000514, 1983.

Klett, J. D.: Stable analytical inversion solution for processing lidar returns, Appl. Optics, 20, 211, 10.1364/ao.20.000211, 1981.

Kroll, J. H., and Seinfeld, J. H.: Chemistry of secondary organic aerosol: Formation and evolution of low-volatility organics in the atmosphere, Atmos. Environ., 42, 3593–3624, doi: 10.1016/j.atmosenv.2008.01.003, 2008.

Kulmala, M., Vehkamaki, H., Petäjä, T., Dal Maso, M., Lauri, A., Kerminen, V.M., Birmili, and W., McMurry, P. H.: Formation and growth rates of ultrafine atmospheric particles: a review of observations, J. Aerosol Sci., 35, 143–176, doi: 10.1016/j.jaerosci.2003.10.003, 2004.

Kumar, P., Andrade, M.F., Ynoue, R.Y., Fornaro, A., de Freitas, E.D., Martins, J., Martins, L.D., Albuquerque, T., Zhang and Y., Morawska, L.: New Directions: From biofuels to wood stoves: the modern and ancient air quality challenges in the megacity of São Paulo, Atmos. Environ., 140, 364–369, 10.1016/j.atmosenv.2016.05.059, 2016.

Kumar, P., Morawska, L., Birmili, W., Paasonen, P., Hu, M., Kulmala, M., Harrison, R.M., Norford, L. and Britter, R.: Ultrafine particles in cities, Environ. Int., 66, 1–10, doi:10.1016/j.envint.2014.01.013, 2014.

Kumar, P., Robins, A., Vardoulakis, S., and Britter, R.: A review of the characteristics of nanoparticles in the urban atmosphere and the prospects for developing regulatory control, Atmos. Environ., 44, 5035–5052, 10.1016/j.atmosenv.2010.08.016, 2010.

Leng, C., Cheng, T., Chen, J., Zhang, R., Tao, J., Huang, G. and Li, L.: Measurements of surface cloud condensation nuclei and aerosol activity in downtown Shanghai, Atmos. Environ., 69, 354–361, doi:10.1016/j.atmosenv.2012.12.021, 2013.

Lim, Y.B., and Ziemann, P.J.: Products and mechanism of secondary organic aerosol formation from reactions of n-alkanes with OH radicals in the presence of NOx, Environ. Sci. Technol., 39, 9229–9236, doi:10.1021/es051447g, 2005.

5 Long, B., Tan, X.F., Wang, Y.B., Li, J., Ren, D.S., and Zhang, W.J.: Theoretical Studies on Reactions of OH with $H_2SO_4^{\cdots}NH_3$ Complex and NH_2 with H_2SO_4 in the Presence of Water, Chemistry Select, 1, 1421–1430, doi:10.1002/slct.201600194, 2016.

Ma, N., and Birmili, W.: Estimating the contribution of photochemical particle formation to ultrafine particle number averages in an urban atmosphere, Sci. Total Environ., 512–513, doi:10.1016/j.scitotenv.2015.01.009, 2015.

10 Marenco, F., V. Santacesaria, A. F. Bais, D. Balis, A. di Sarra, A. Papayannis, and C. Zerefos.: Optical properties of tropospheric aerosols determined by lidar and spectrophotometric measurements (Photochemical Activity and Solar Ultraviolet Radiation campaign), Appl. Optics, 36, 6875–6886, doi:10.1364/AO.36.006875, 2002.

Mcfiggans, G., Artaxo, P., Baltensperger, U., Coe, H., Facchini, M. C., Feingold, G., and Paulo, C.E.P.S.: The effect of physical and chemical aerosol properties on warm cloud droplet activation, Atmos. Chem. Phys., 6, 2593–2649,
15 doi:10.5194/acp-6-2593-2006, 2006.

Metzger, A., Verheggen, B., Dommen, J., Duplissy, J., Prevot, A. S. H., Weingartner, E., Riipinenc, I., Kulmalac, M., Spracklend, D. V., Carslawd, K. S., and Baltensperger, U.: Evidence for the role of organics in aerosol particle formation under atmospheric conditions, Proc. Natl. Acad. Sci. U. S. A, 107, 6646–51, doi:10.1073/pnas.0911330107, 2010.

Monks, P. S., Archibald, A. T., Colette, A., Cooper, O., Coyle, M., Derwent, R., Fowler, D., Granier, C., Law, K.S., Mills,
20 G.E., Stevenson, D.S., Tarasova, O., Thouret, V., Von Schneidemesser, E., Sommariva, R., Wild, O., and Williams, M.L.: Tropospheric ozone and its precursors from the urban to the global scale from air quality to short-lived climate forcer, Atmos. Chem. Phys., 15, 8889–8973, doi:10.5194/acp-15-8889, 2015.

Müller, D., Ansmann, A., Mattis, I., Tesche, M., Wandinger, U., Althausen, D., and Pisani, G.: Aerosol-type-dependent lidar ratios observed with raman lidar, J. Geophys. Res., 112, D16202, doi:10.1029/2006jd008292, 2007.

25 Nie, W., Ding, A., Wang, T., Kerminen, V.-M., George, C., Xue, L., and Kulmala, M.: Polluted dust promotes new particle formation and growth, nature, 4, 6634, doi:10.1038/srep06634, 2014.

Ortega, A. M., Hayes, P. L., Peng, Z., Palm, B. B., Hu, W., Day, D. A., Li, R., Cubison, M.J.,Brune, W. H., Graus, M., Warneke, C., Gilman, J.B., Kuster, W.C., Gouw, J, Gutiérrez-Montes, C., and Jimenez, J. L.: Real-time measurements of secondary organic aerosol formation and aging from ambient air in an oxidation flow reactor in the Los Angeles area,
30 Atmos. Chem. Phy., 15, 21907–21958, doi:10.5194/acpd-15-21907, 2015.

Oyama, B. S., Andrade, M. F., Herckes, P., Dusek, U., Röckmann, T., and Holzinger, R.: Vehicular emissions of organic particulate matter in Sao Paulo, Brazil, Atmos. Chem. Phy. Disc., 15, 33755–33788. doi:10.5194/acpd-15-33755, 2015.

Papayannis, A., and Chourdakis, G.: The EOLE Project: A multiwavelength laser remote sensing (lidar) system for ozone and aerosol measurements in the troposphere and the lower stratosphere. Part II: Aerosol measurements over Athens, Greece,

International Journal of remote Sensing, 23, 179–196, doi:10.1080/01431160010025952, 2002.

Paramonov, M., Aalto, P. P., Asmi, a., Prisle, N., Kerminen, V. M., Kulmala, M., and Petäjä, T.: The analysis of size-segregated cloud condensation nuclei counter (CCNC) data and its implications for cloud droplet activation. Atmos. Chem. Phys., 13, 10285–10301, doi:10.5194/acp-13-10285-2013, 2013.

5 Peng, J. F., Hu, M., Wang, Z.B., Huang, X.F., Kumar, P., Wu, Z.J., and He, L.Y.: Submicron aerosols at thirteen diversified sites in China: size distribution, new particle formation and corresponding contribution to cloud condensation nuclei production, Atmos. Chem. Phys., 14, 10249–10265, doi:10.5194/acp-14-10249-2014, 2014.

Pierce, J. R., Leaitch, W. R., Liggio, J., Westervelt, D. M., Wainwright, C. D., Abbatt, J. P. D., Ahlm, L., Al-Basheer, W., Cziczo, D. J., Hayden, K. L., Lee, A. K. Y., Li, S.M., Russell, L. M., Sjostedt, S. J., Strawbridge, K. B., Travis, M.,
10 Vlasenko, A., Wentzell, J. J. B., Wiebe, H. A., Wong, J. P. S. and MacDonald, A. M.: Nucleation and condensational growth to CCN sizes during a sustained pristine biogenic SOA event in a forested mountain valley, Atmos. Chem. Phys., 12, 3147–3163. doi:10.5194/acp-12-3147, 2012.

Quinn, P. K., Bates, T. S., Coffman, D. J., and Covert, D. S.: Influence of particle size and chemistry on the cloud nucleating properties of aerosols, Atmos. Chem. Phys., 7, 14171–14208, doi: 10.5194/acp-8-1029-2008, 2008.

15 Reade, L., Jennings, S. G., and McSweeney, G.: Cloud condensation nuclei measurements at Mace Head, Ireland, over the period 1994–2002, Atmos. Res., 82, 610–621, doi10.1016/j.atmosres.2006.02.017, 2006.

Reche, C., Querol, X., Alastuey, A., Viana, M., Pey, J., Moreno, T., Rodrıguez, S., Gonzalez, Y., Fernández-Camacho, R., Sánchez de la Campa, A. M., De la Rosa, J., Dall'Osto, M., Prévôt, A. S. H., Hueglin, C., Harrison, R. M., and Quincey, P.: New considerations for PM, Black Carbon and particle number concentration for air quality monitoring across different
20 European cities, Atmos. Chem. Phys., 11, 6207–6227, doi:10.5194/acp-11-6207, 2011.

Remer, L. A., Kaufman, Y. J., Tanré, D., Mattoo, S., Chu, D. A., Martins, J. V., Li, R. R., Ichoku, C., Levy, R. C., Kleidman, R. G., Eck, T. F., Vermote, E., and Holben, B. N.: The MODIS aerosol algorithm, products, and validation, J. Atmos. Sci., 62, 947–973, doi:10.1175/JAS3385.1, 2005.

Reff, A., Eberly, S. I., and Bhave, P. V.: Receptor Modeling of Ambient Particulate Matter Data Using Positive Matrix
25 Factorization.: Review of Existing Methods Receptor Modeling of Ambient Particulate Matter Data Using Positive Matrix Factorization, J. Air Waste Manag. Assoc., 57, 146-154, doi:10.1080/10473289.2007.10465319, 2007

Riipinen, I., Pierce, J. R., Yli-Juuti, T., Nieminen, T., Häkkinen, S., Ehn, M., Junninen, H., Lehtipalo, K., Petäjä, T., Slowik, J., Chang, R., Shantz, N.C., Abbatt, J., Leaitch, W.R., Kerminen, V.M., Worsnop, D.R., Pandis,S. N., Donahue, N. M. and Kulmala, M.: Organic condensation: A vital link connecting aerosol formation to cloud condensation nuclei (CCN)
30 concentrations, Atmos. Chem. Phys., 11, 3865–3878. doi:10.5194/acp-11-3865, 2011.

Roberts, G. C., and Nenes, A.: A Continuous-Flow Streamwise Thermal-Gradient CCN Chamber for Atmospheric Measurements, Aerosol Sci. Technol., 39, 206–221, doi: 10.1080/027868290913988, 2005.

Rodrigues, P.F., Landulfo, E., Gandu, A. W., and Lopes, F.J.S.: Assessment of aerosol hygroscopic growth using an elastic LIDAR and BRAMS simulation in urban metropolitan areas, AIP Conf. Proc., 1531, 360, doi:10.1063/1.4804781, 2013.

Sanchez-Ccoyllo, O. R., and Andrade, M. F.: The influence of meteorological conditions on the behavior of pollutants concentrations in São Paulo, Brazil, Environ. Pollut., 116, 257–263, doi:10.1016/S0269-7491(01)00129-4, 2002.

Sánchez-Ccoyllo, O. R., Ynoue, R.Y., Martins, L.D., Astolfo, R., Miranda, R.M., Freitas, E.D., Borges, A.S., Fornaro, A., Freitas, H., Moreira, A., and Andrade, M.F.: Vehicular particulate matter emissions in road tunnels in São Paulo, Brazil, Environmental Monit. Assess., 149, 241–249. doi:10.1007/s10661-008-0198-5, 2008.

Sasano, Y., and Nakane, H.: Significance of the extinction/backscatter ratio and the boundary value term in the solution for the two-component lidar equation, Appl. Opt., 23, 1-13, doi:10.1364/AO.23.0011_1, 1984.

Seinfeld, J.H. and Pandis, S.N.: Atmospheric chemistry and physics: from air pollution to climate change, John Wiley and Sons, New York, 2006.

Shilling, J. E., Zaveri, R. A., Fast, J. D., Kleinman, L., Alexander, M. L., Canagaratna, M. R., Fortner, E., Hubbe, J. M., Jayne, J. T., Sedlacek, A., Setyan, A., Springston, S., Worsnop, D. R., and Zhang, Q.: Enhanced SOA formation from mixed anthropogenic and biogenic emissions during the CARES campaign, Atmos. Chem. Phys., 13, 2091–2113, doi:10.5194/acp-13-2091, 2013.

Sihto, S.L., Mikkilä, J., Vanhanen, J., Ehn, M., Liao, L., Lehtipalo, K., and Kulmala, M.: Seasonal variation of CCN concentrations and aerosol activation properties in boreal forest, Atmos. Chem. Phys., 11, 13269–13285, doi:10.5194/acp-11-13269-2011, 2011.

Silva, M.F., Assunção, J.V., Andrade, M.F., and Pesquero, C.: Characterization of metal and trace element contents of particulate matter (PM10) emitted by vehicles running on Brazilian fuels—hydrated ethanol and gasoline with 22% of anhydrous ethanol, J. Toxicol. Environ. Health, A73, 901–909, doi:10.1080/15287391003744849, 2010.

Sorribas, M., Adame, J. a, Olmo, F. J., Vilaplana, J. M., Gil-Ojeda, M., and Alados-Arboledas, L.: A long-term study of new particle formation in a coastal environment: meteorology, gas phase and solar radiation implications, Sci. Total Environ., 511, 723–37, doi:10.1016/j.scitotenv.2014.12.011, 2015.

Taiwo, A. M., Harrison, R. M., and Shi, Z.: A review of receptor modelling of industrially emitted particulate matter, Atmos. Environ., 97, 109–120, doi:10.1016/j.atmosenv.2014.07.051, 2014.

Vara-Vela, A., Andrade, M. F., Kumar, P., Ynoue, R. Y., and Muñoz, A. G.: Impact of vehicular emissions on the formation of fine particles in the Sao Paulo Metropolitan Area: a numerical study with the WRF-Chem model, Atmos. Chem. Phys., 16, 777–797, doi:10.5194/acp-16-777-2016, 2016.

Wallington, T.J., Anderson, J., Kurtz, E. M., and Tennison P.J.: Biofuels, vehicle emissions, and urban air quality, Faraday Discuss, 189, 121, doi:10.1039/c5fd00205b, 2016.

Wu, Z., Hu, M., Liu, S., Wehner, B., Bauer, S., Wiedensohler, A., Petäjä, T., DalMaso, M., and Kulmala, M.: New particle formation in Beijing, China: statistical analysis of a 1-year data set, J. Geophys. Res., 112, D09209, doi:10.1029/2006jd007406, 2007.

Yuan, B., Hu, W. W., Shao, M., Wang, M., Chen, W. T., Lu, S. H., Zeng, M. and Hu, M.: VOC emissions, evolutions and contributions to SOA formation at a receptor site in eastern China, Atmos. Chem. Phys., 13, 8815–8832, doi:10.5194/acp-

13-8815, 2013.

Yue, D. L., Hu, M., Zhang, R. Y., Wu, Z. J., Su, H., Wang, Z. B., and Wiedensohler, A.: Potential contribution of new particle formation to cloud condensation nuclei in Beijing, Atmos. Environ., 45, 6070–6077, doi:10.1016/j.atmosenv.2011.07.037, 2011.

5 Yum, S.S., James, G.H., Keun, Y.S., and Byoung-Cheol, C.: Springtime cloud condensation nuclei concentrations on the west coast of Korea, Geophys. Res. Lett., 32, L09814, doi:10.1029/2005gl022641, 2005.

Zhang, F., Li, Y., Li1, Z., Sun, L., Li, R., Zhao, R., Wang, P., Sun, Y., Liu, X., Li, J., Li, P., Ren, G., and Fan, T.: Aerosol hygroscopicity and cloud condensation nuclei activity during the AC3Exp campaign: implications for cloud condensation nuclei parameterization, Atmos. Chem. Phys., 14, 13423–13437, doi:10.5194/acpd-14-14889-2014, 2014.

10 Zhang, R., Suh, I., Zhao, J., Zhang, D., Fortner, E.C., Tie, X., Molina, L.T., and Molina, M.J.: Atmospheric new particle formation enhanced by organic acids, Science, 304, 1487–1490, doi:10.1126/science.1095139, 2004.

Zhang, R., Wang, L., Khalizov, A.F., Zhao, J., Zheng, J., McGraw, R.L., and Molina, L.T.: Formation of nanoparticles of blue haze enhanced by anthropogenic pollution, Proc. Natl. Acad. Sci. U.S.A, 106, 17650–17654, doi:10.1073/pnas.0910125106, 2009.

15 Zhu, Y., Sabaliauskas, K., Liu, X., Meng, H., Gao, H., Jeong, C.H., Evans, G.J., and Yao, X.: Comparative analysis of new particle formation events in less and severely polluted urban atmosphere, Atmos. Environ., 98, 655–664, doi:10.1016/j.atmosenv.2014.09.043, 2014.

Table 1. Daytime data for meteorological parameters (temperature, relative humidity and rain), particle number concentration and cloud condensation nuclei during the period evaluated (19 August to 3 September, 2014). Peak diameter was calculated by size distribution mode. The last column, represent periods with NPF events and remote sources influence on MASP atmosphere.

Day		Date	Temperature (°C) mean (range)	RH (%) mean (range)	Rain (mm)	PNC (cm^{-3}) mean ± SD	(range)	Dp (nm)	Cloud Condensation Nuclei (mean ± SD)					Remote Source* and NPF	
									SS = 0.2%	SS = 0.4%	SS = 0.6%	SS = 0.8%	SS = 1.0%	Daytime	Nighttime
1	Tue	8/19/14	15 (11 - 20)	83 (64 - 96)	0.0	7654 ± 4582	1874 - 16607	50	1688 ± 569	1809 ± 624	2270 ± 830	2555 ± 965	2811 ± 1029		
2	Wed	8/20/14	16 (11 - 23)	80 (43 - 98)	0.0	13086 ± 8242	3335 - 35398	45	2240 ± 780	2385 ± 961	2969 ± 1191	3431 ± 1371	3770 ± 1611		
3	Thu	8/21/14	18 (13 - 27)	70 (32 - 95)	0.0	14133 ± 7647	3360 - 27144	54	2683 ± 1019	3082 ± 1451	3726 ± 1715	4201 ± 1831	4562 ± 1933		
4	Fri	8/22/14	19 (12 - 28)	62 (30 - 92)	0.0	15921 ± 7935	5529 - 35508	73	3368 ± 2664	2487 ± 1034	3208 ± 1512	3699 ± 1766	3960 ± 1890		[blue]
5	Sat	8/23/14	20 (13 - 28)	58 (28 - 87)	0.0	15923 ± 7644	5595 - 32061	72	3889 ± 752	4708 ± 1309	5633 ± 1588	6296 ± 1800	6860 ± 1894		
6	Tue	8/26/14	19 (16 - 23)	76 (48 - 96)	1.3	13091 ± 4965	5758 - 26105	92	2765 ± 411	5135 ± 1908	5961 ± 2242	6343 ± 2336	6678 ± 2522	[red]	[red]
7	Wed	8/27/14	15 (10 - 20)	79 (55 - 93)	0.1	8627 ± 4965	1924 - 20416	50	1103 ± 549	1444 ± 954	1822 ± 1304	2229 ± 1405	2507 ± 1592	[orange]	[blue]
8	Thu	8/28/14	13 (10 - 18)	84 (62 - 96)	0.0	11313 ± 6449	4920 - 25556	42	1432 ± 438	2103 ± 1181	2672 ± 1388	3117 ± 1536	3538 ± 1702	[orange]	
9	Fri	8/29/14	13 (12 - 16)	85 (74 - 91)	0.0	9873 ± 3751	5170 - 17513	37	1609 ± 275	2201 ± 529	2747 ± 723	3146 ± 823	3444 ± 861		
10	Sat	8/30/14	16 (12 - 22)	80 (48 - 94)	0.0	12601 ± 8315	4486 - 30528	53	1945 ± 384	3144 ± 1142	3856 ± 1380	4304 ± 1632	4734 ± 1743	[orange]	
11	Sun	8/31/14	18 (14 - 30)	83 (30 - 96)	2.2	7078 ± 4543	2781 - 18794	63	1573 ± 679	2144 ± 998	2525 ± 1159	2800 ± 1277	3036 ± 1366		
12	Mon	9/1/14	19 (15 - 26)	75 (48 - 95)	0.1	11014 ± 8580	2196 - 31674	38	782 ± 661	1315 ± 1011	1959 ± 1273	2336 ± 1263	2757 ± 1510	[red]	
13	Tue	9/2/14	19 (14 - 27)	79 (46 - 96)	3.6	14842 ± 10075	2294 - 32152	67	2138 ± 661	3861 ± 1564	4718 ± 1922	5281 ± 2073	5757 ± 2135	[red]	
14	Wed	9/3/14	18 (15 - 25)	80 (57 - 96)	2.2	7713 ± 7303	1347 - 26928	29	609 ± 328	727 ± 428	981 ± 580	1237 ± 701	1523 ± 834	[orange]	
Mean	-	-	17 (10 - 30)	79 (28 - 98)	0.9	11634 ± 3077	1347 - 35508	55	1987 ± 942	2610 ± 1264	3218 ± 1435	3641 ± 1512	3996 ± 1572		

RH – relative humidity; PNC – particle number concentration; Dp – peak diameter; NPF – new particle formation; SS – supersaturation; SD – standard deviation.

Days with NPF events [orange]

* Vehicular traffic is considered the main source during daytime period in all days.

Remote source apportionment

Sea salt + industrial [blue]	Biomass burning + vehicular [red]

Table 2. Comparison of mean activation ratio and particle number concentration (at different supersaturation levels) observed in this study and in other studies. In our study the values were separated for daytime and nighttime.

Reference		Site	Environment	Details	Activated ratio (CCN/PNC)*					PNC (x10⁴) cm⁻³
					0.20%	0.40%	0.60%	0.80%	1.0%	
This study	Total mean	Sao Paulo	Urban	Entire campaign	0.19±0.12	0.24±0.16	0.30±0.19	0.35±0.20	0.38±0.22	1.2±0.77
	Diurnal			-	0.13±0.08	0.16±0.09	0.19±0.10	0.22±0.11	0.52±0.21	1.6±0.78
	Nocturnal			-	0.24±0.12	0.33±0.15	0.41±0.18	0.47±0.19	0.24±0.12	0.3±0.69
Almeida et al.(2014)		Sao Paulo	Urban	Entire campaign	0.10±0.05	0.19±0.09	0.23±0.10	0.26±0.11	0.28±0.12	1.3±0.54
Andreae et al.(2004)		Amazon	Forest	Green ocean	-	-	-	-	0.68	0.05
Leng et al.(2013)		Shangai	Urban/Coast	Continental - Marine	-	-	-	0.4 and 0.6	-	0.5 - 1.0
Gunthe et al.,(2011)		Beijing	Urban	Entire camapaign	0.41±0.21	0.54±0.21	0.60±0.23	0.66±0.23	-	1.7±0.4
				Aged pollution	0.62±0.08	0.74±0.08	0.80±0.08	0.84±0.06	-	1.1±0.23
				Fresh city pollution	0.15±0.12	0.25±0.21	0.34±0.24	0.42±0.26	-	1.2±0.37
Burkart et al.(2011)		Vienna	Urban	SS = 0.5%	-	0.13	-	-	-	0.9 - 5.4
Sihto et al.(2011)		Finland	Forest	-	-	0.21 - 0.42	-	-	-	~0.2
Yum et al.(2005)		Korea	Urban/Coast	Continental - Marine	-	-	-	-	0.43 - 0.74	0.4 - 0.8
Furutani et al.(2008)		California	Urban/Coast	Anthropogenic polluted	-	-	0.4 - 0.6[e]	-	-	0.2 - 1.5
				Fresh Ship exaust	-	-	0.06 - 0.2	-	-	1.5 - 3.0
		Pacific Ocean	Over Ocean	-	-	-	0.6 - 1.0	-	-	0.2 - 0.6

* CCN – cloud condensation nuclei; PNC – particle number concentration; SS – supersaturation.
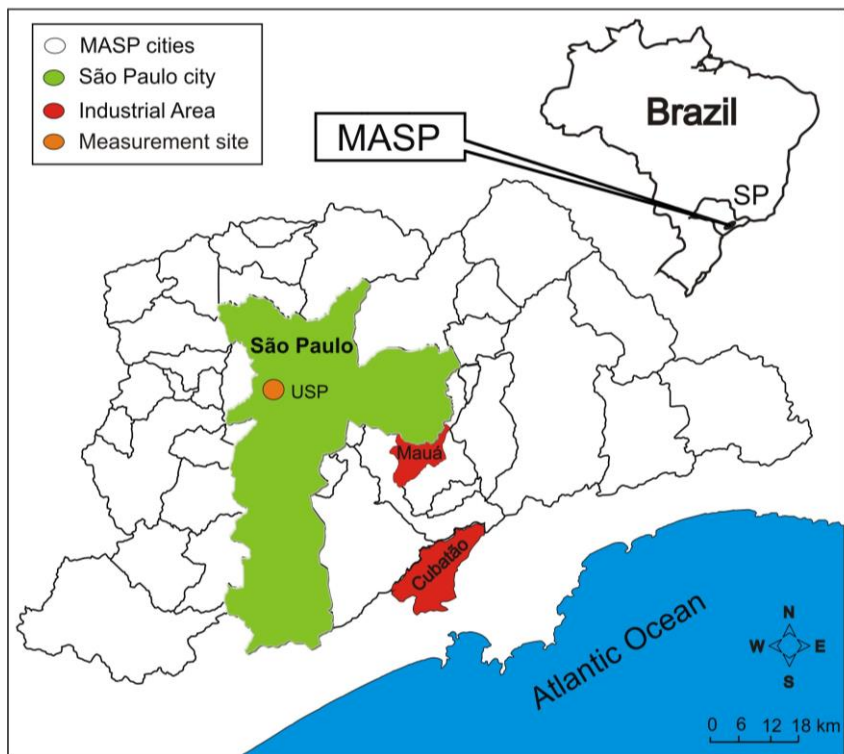
Figure 1. Map of Metropolitan Area of São Paulo (MASP). The city of São Paulo proper appears in green. Measurement and sampling sites are located on the campus of the University of São Paulo, represented by an orange circle. The cities of Cubatão and Mauá, both of which comprise large industrial areas appear in red.
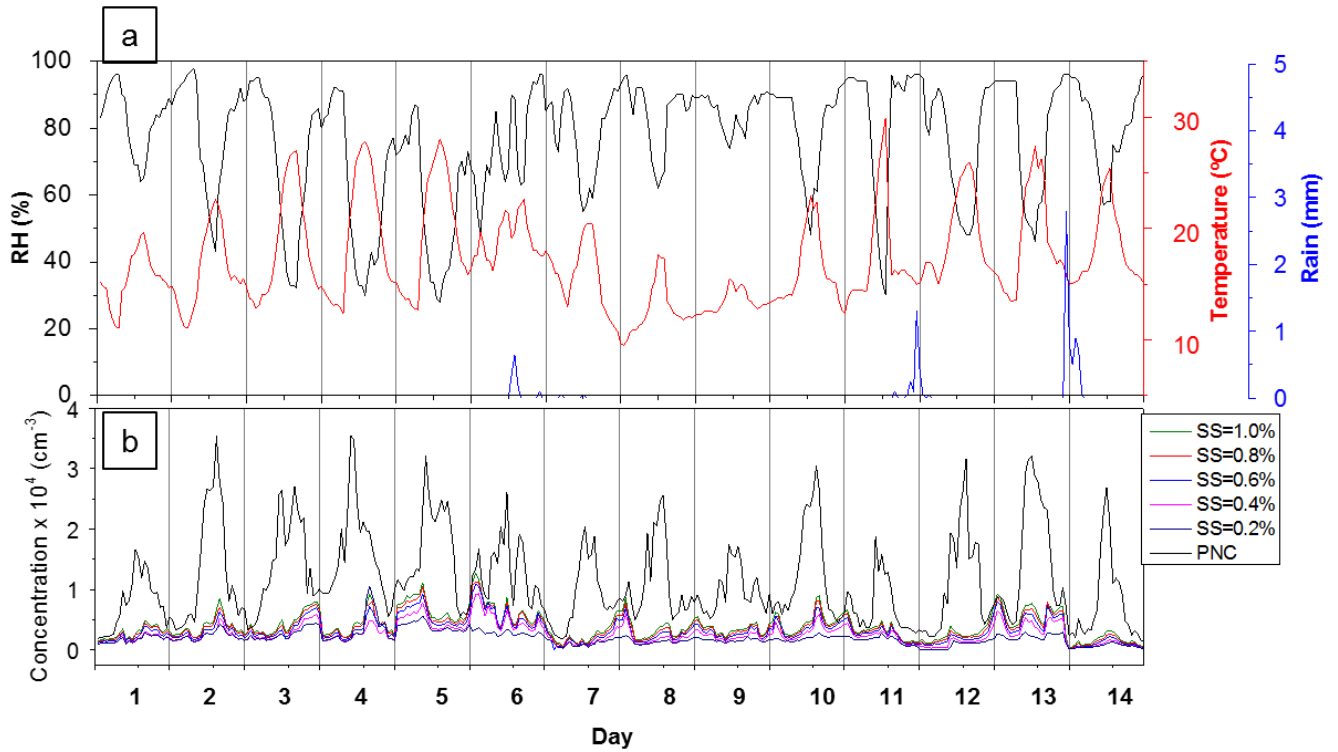
Figure 2. Hourly variability in(a) meteorological parameters such as relative humidity (RH), temperature and rainfall, and also for (b) particle number concentration (PNC) and cloud condensation nuclei (CCN) for the studied period. Note that the PNC corresponds to a size distribution of 9–1000 nm, whereas the CCN correspond to a size distribution of 10–2500 nm.
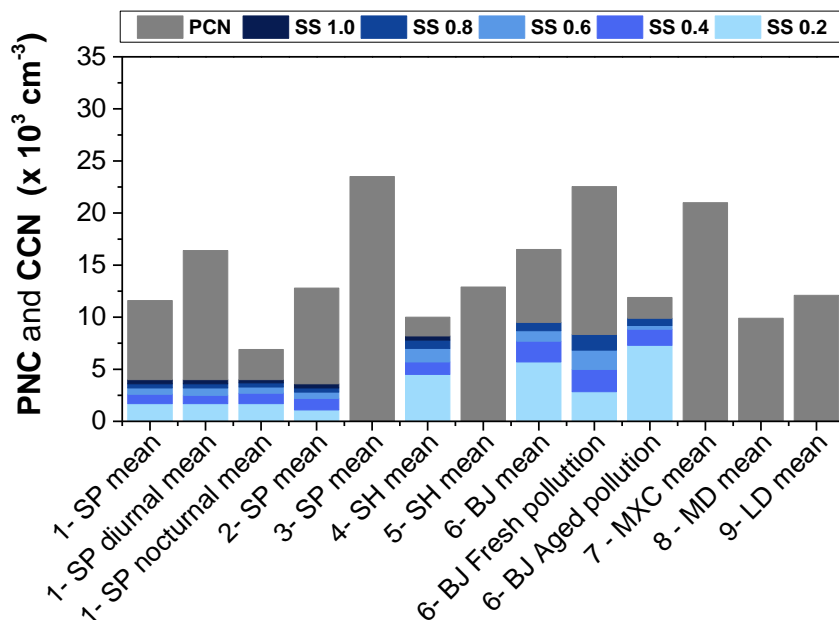
Figure 3. Comparison between particle number concentration (PNC) and cloud condensation nuclei (CCN) values obtained in this study and in previous studies. All studies were carried out at urban background monitoring sites, where measurements were made on rooftops of buildings located some kilometres from the downtown areas. In the case of Toronto, the measurements were carried in the downtown area of the city. Detailed information is available on Supplementary Information in Table S1.

SP – São Paulo; SH – Shangai; BJ – Beijing; MXC – Mexico City; MD – Madrid; LD – London; 1 –the present study; 2 –Almeida et al. (2014); 3 – Backman et al. (2012); 4 –Leng et al. (2013); 5 – Peng et al. (2014); 6 –Gunthe et al. (2011); 7 – Kalafut-Pettibone et al. (2011); 8 – Gómez-Moreno et al. (2011); 9 –Reche et al. (2011).
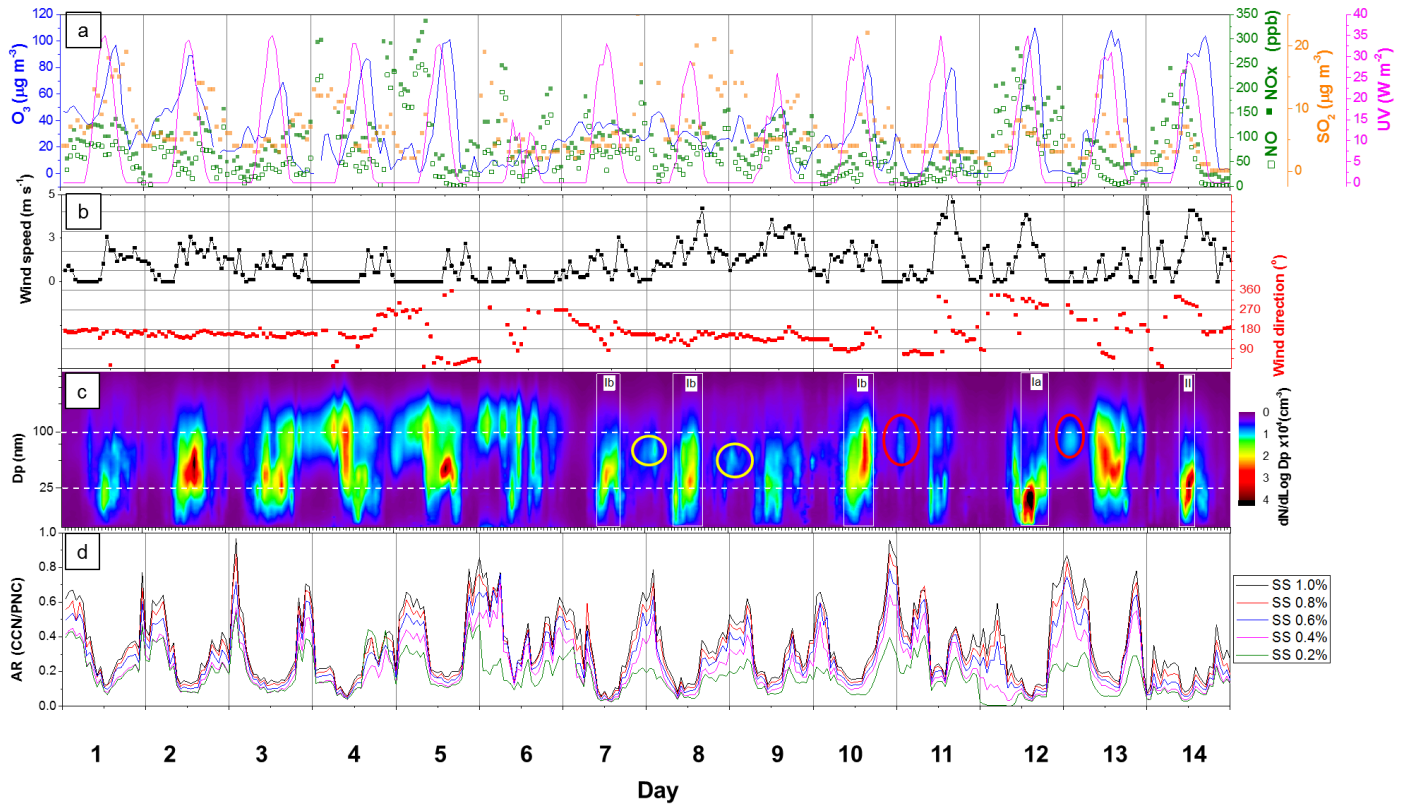
Figure 4. Hourly variability for (a) UV radiation, together with concentrations of SO₂, NOₓ, NO₂and O₃; (b) wind direction and speed; (c) particle number distribution (yellow and red circles indicate conditions of low- and high-O₃ concentrations, respectively); and (d) activation ratio (AR), representing the cloud condensation nuclei/particle number concentration (CCN/PNC) ratio. UV radiation data, as well as the concentrations of SO₂, O₃, NOₓ and NO₂, were provided by the São Paulo State Environmental Protection Agency.
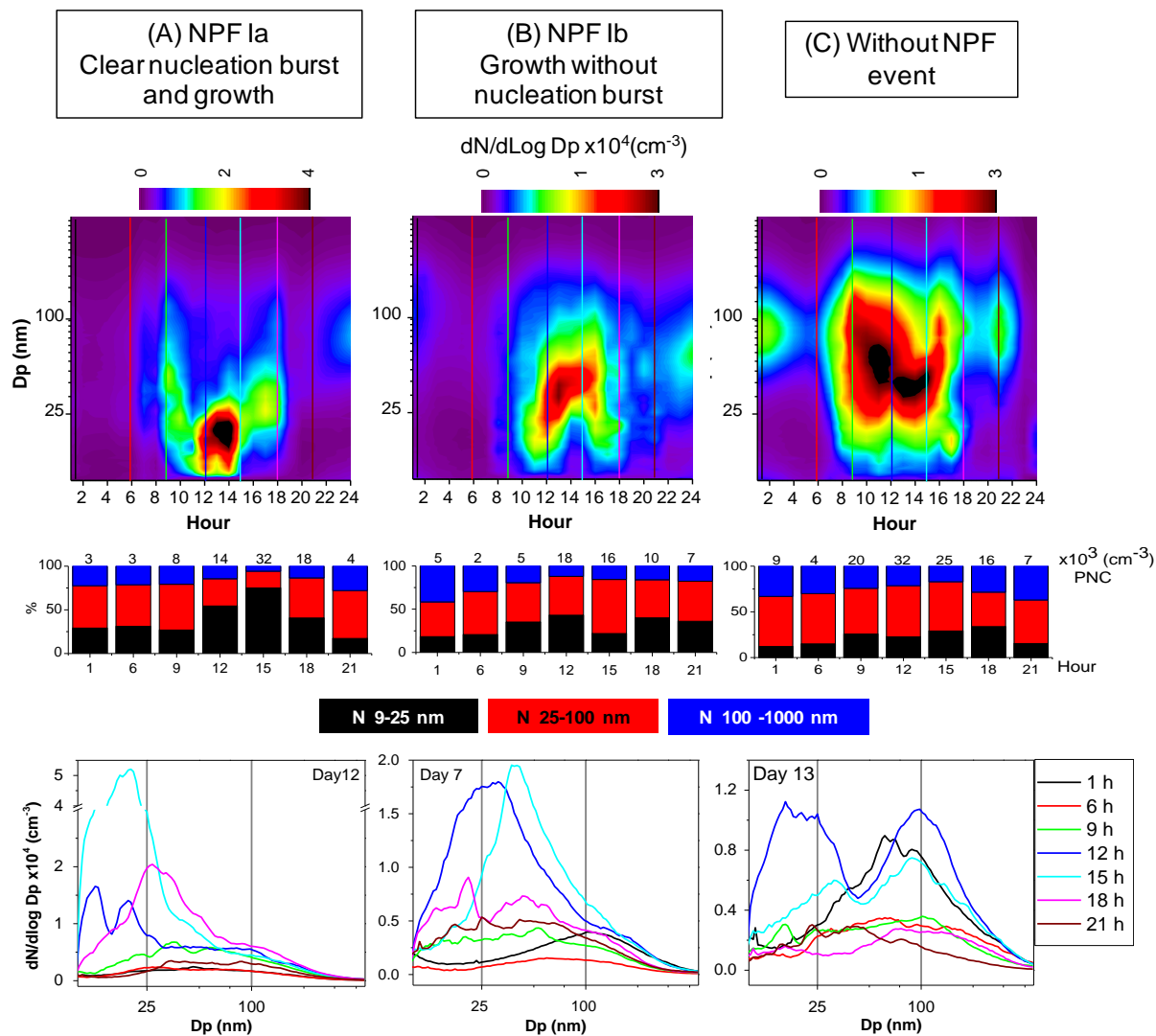
Figure 5. Particle number distribution (PND) contour plots for days with (a) new particle formation (NPF) events categorised as class Ia; (b) class Ib NPF events; and (c) no NPF events. The hourly bars show the proportions of particle number concentrations (PNCs) in three modes (nucleation, Aitken and accumulation) and hourly line graphs show PND distribution. Selected hours were marked on the PND contour plots in order to compare them with the hourly PND line graphs.
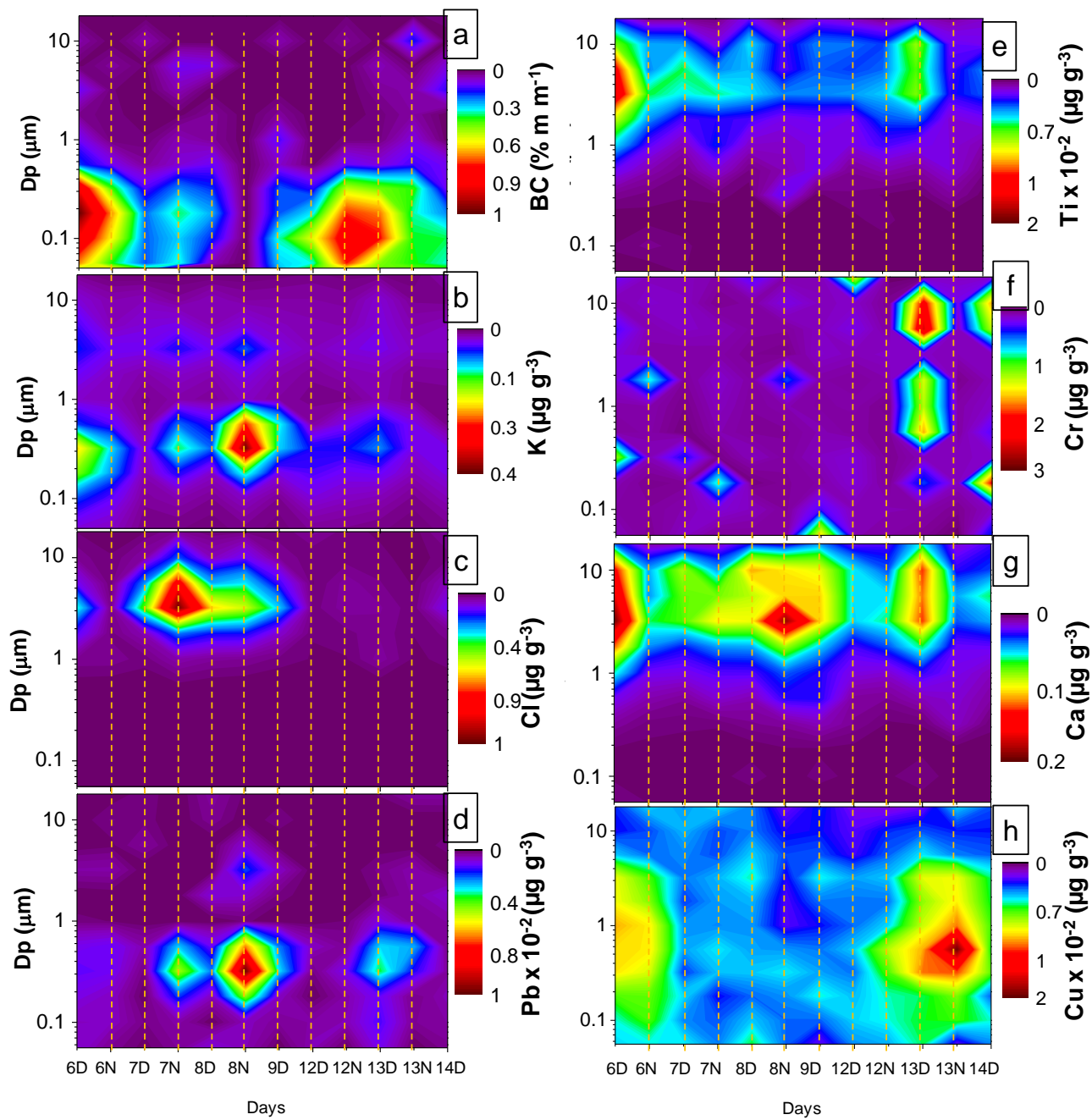
Figure 6. Mass size distribution of elemental concentrations of aerosol samples collected by Micro-orifice Uniform Deposit Impactor (a–h) during the daytime period (0700–1900h) and nighttime period (1900–0700 h), represented by D and N, respectively. All sampling days were weekdays.
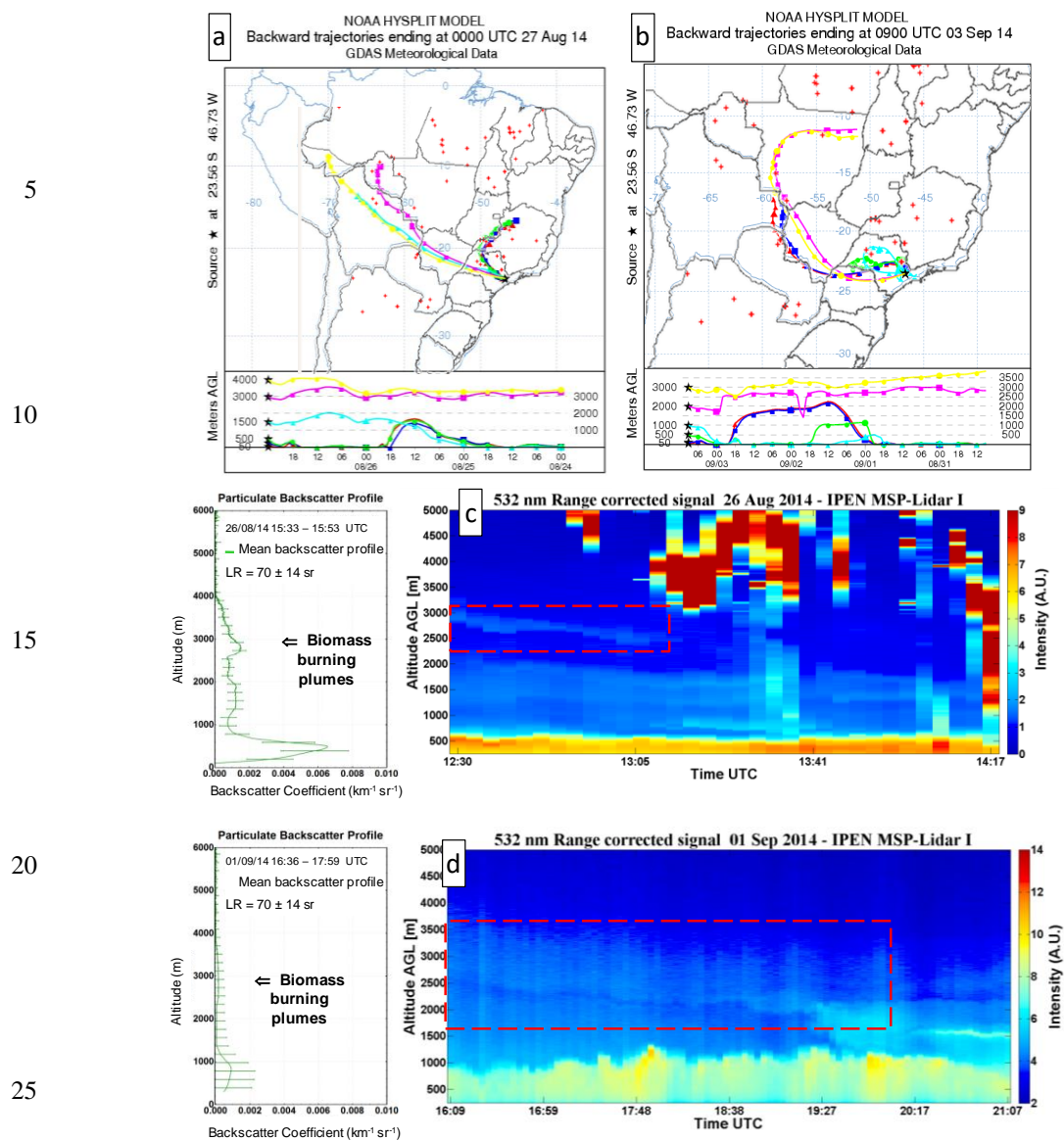
Figure 7. Trajectory and lidar analyses for days with biomass-burning events. (a,b) Hybrid Single Particle Lagrangian Integrated Trajectory (HYSPLIT) trajectory models and biomass-burning events for days 6, 7, 12, 13 and 14. (c,d) The particulate backscatter profile and lidar analyses for days 6 and 12, when the prevailing wind was from the north or north-east, where most biomass-burning events occur. The biomass-burning plumes were detected by lidar and Geostationary Operational Environmental Satellite.

NOAA – (United States) National Oceanic and Atmospheric Administration; GDAS – Global Data Assimilation System; AGL – above ground level; IPEN – *Instituto de Pesquisas Energéticas e Nucleares* ([Brazilian] Nuclear and Energy Research Institute); MSP-Lidar I – Lidar I of the Municipality of São Paulo; LR – lidar ratio.
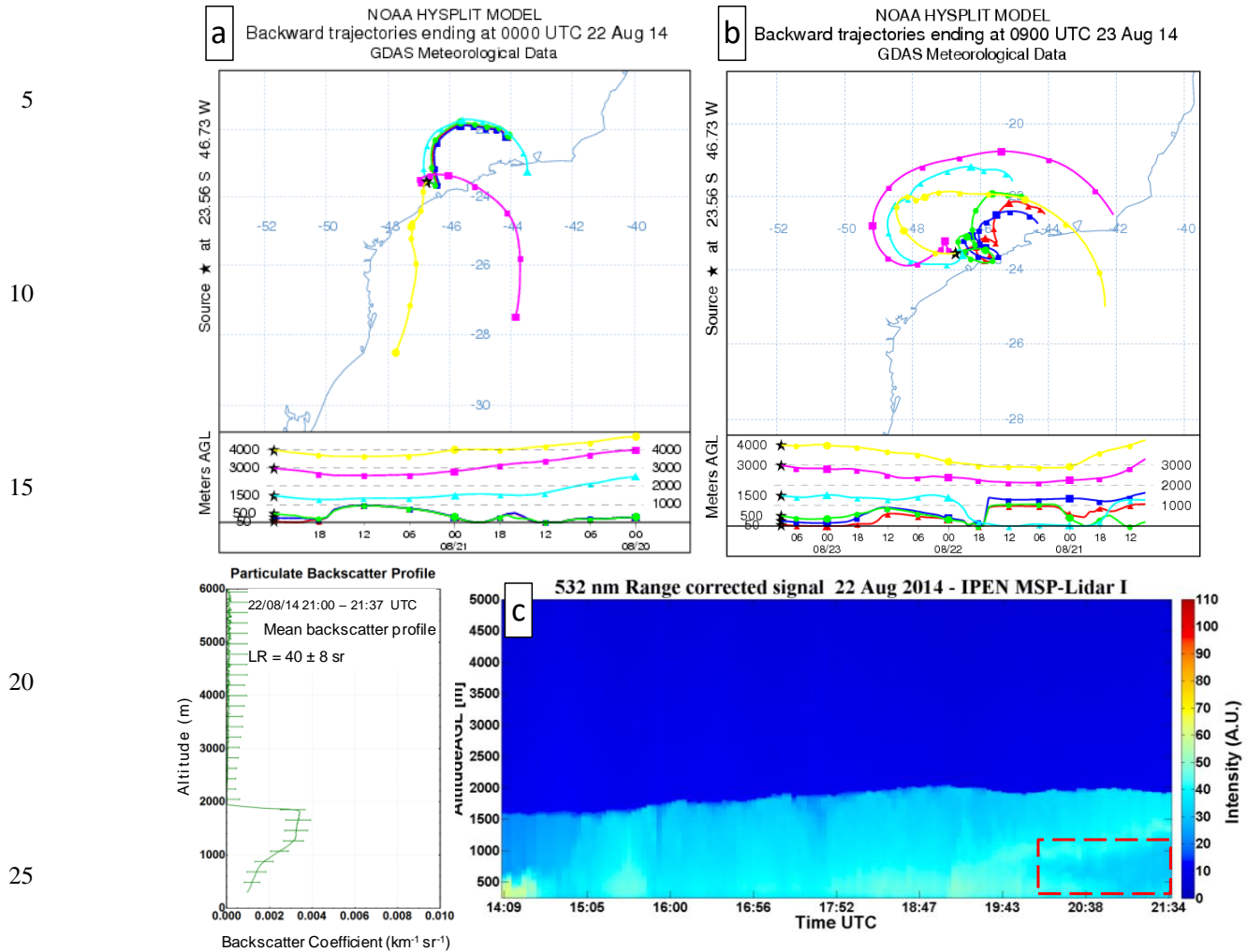
Figure 8. Trajectory and lidar analyses for days with sea-salt apportionment. (a,b) Hybrid Single Particle Lagrangian Integrated Trajectory (HYSPLIT) trajectory models for days 3, 4 and 5. (c) Particulate backscatter profile and lidar analyses for days 3 and 4, when the prevailing wind was from the south, south-east or south-west (i.e. from the Atlantic Ocean and coastal regions). Sea-salt plumes were detected by lidar analysis on day 4, although higher confidence interval concentrations were observed on days 7 and 8.

NOAA – (United States) National Oceanic and Atmospheric Administration; GDAS – Global Data Assimilation System; AGL – above ground level; IPEN – *Instituto de Pesquisas Energéticas e Nucleares* ([Brazilian] Nuclear and Energy Research Institute); MSP-Lidar I – Lidar I of the Municipality of São Paulo; LR – lidar ratio.
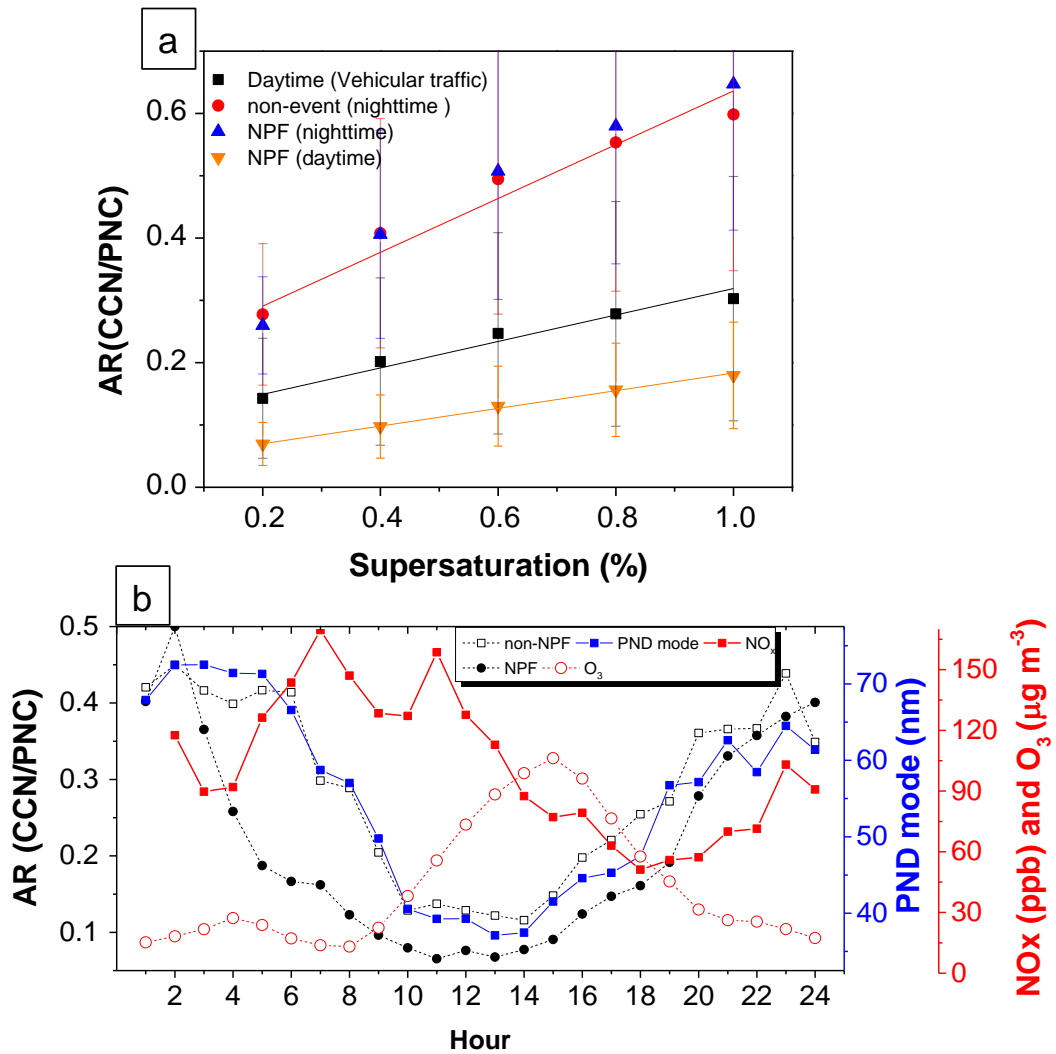
Figure 9. (a) Mean activation ratio (AR) for the daytime (vehicular traffic) and nighttime periods of days with and without new particle formation (NPF) events, by level of supersaturation. (b) Mean hourly AR (at a supersaturation of 0.4%) on days with and without NPF events, plotted together with particle size mode, nitrogen oxides (NO_x) and O_3 in order to evaluate the effect of vehicular emissions on particle size and AR. The AR values for nighttime and daytime showed clear differences, whereas days with NPF events presented slightly lower values than did days without. Two processes contribute to particle size and AR decrease, namely primary aerosol from vehicular traffic (NO_x) and secondary NPF formed in the afternoon.

PND – particle number distribution.
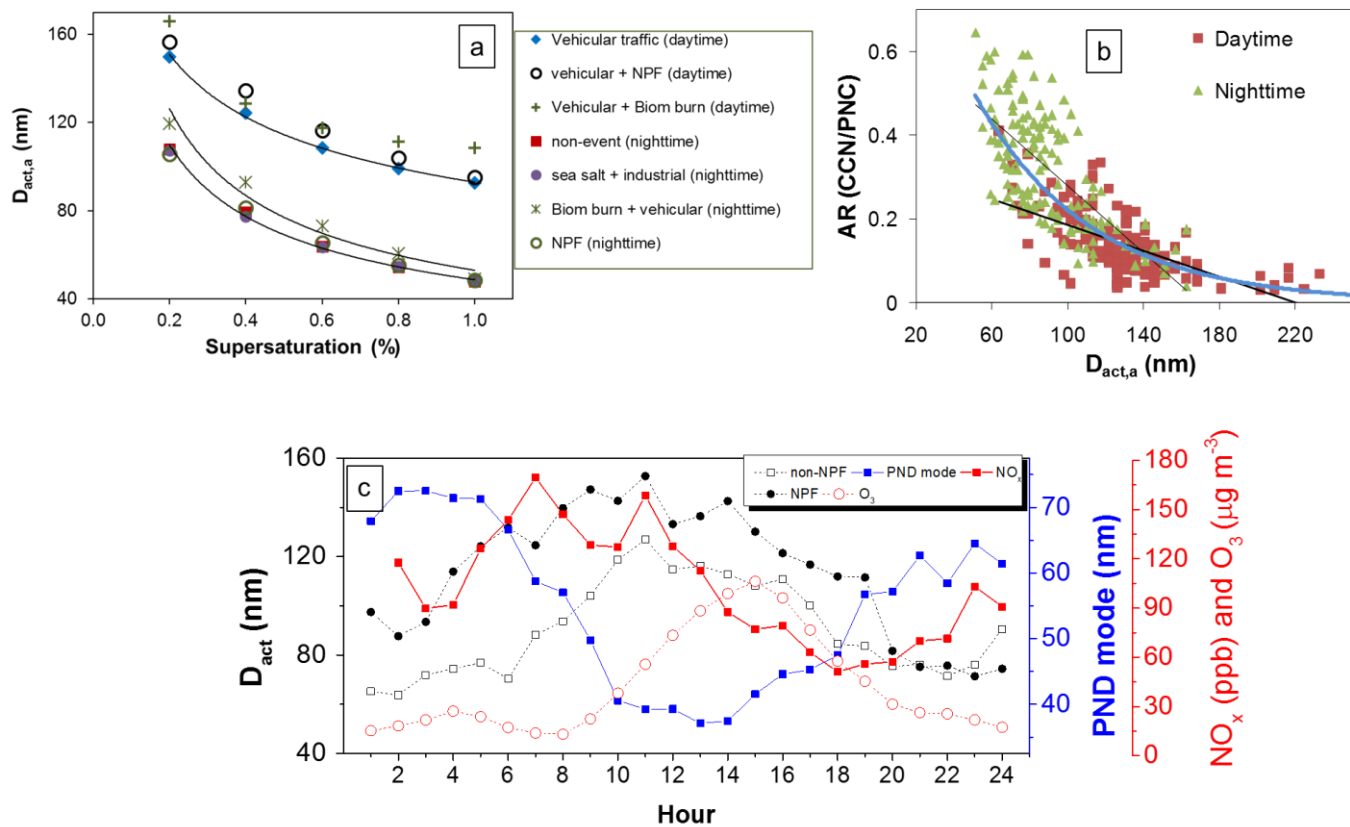
5 **Figure 10.** (a) Mean apparent activation diameter (D_{act}) at various supersaturation levels, showing that it was highest at the lower levels of supersaturation. (b) Activation ratio (AR), in relation to the D_{act}. (c). Time series of D_{act} on days with and without new particle formation (NPF) events, plotted together with particle size mode, NO_x and O_3. The D_{act} values were calculated for supersaturation of 0.4%. Biom burn – biomass burning; PND – particle number distribution.
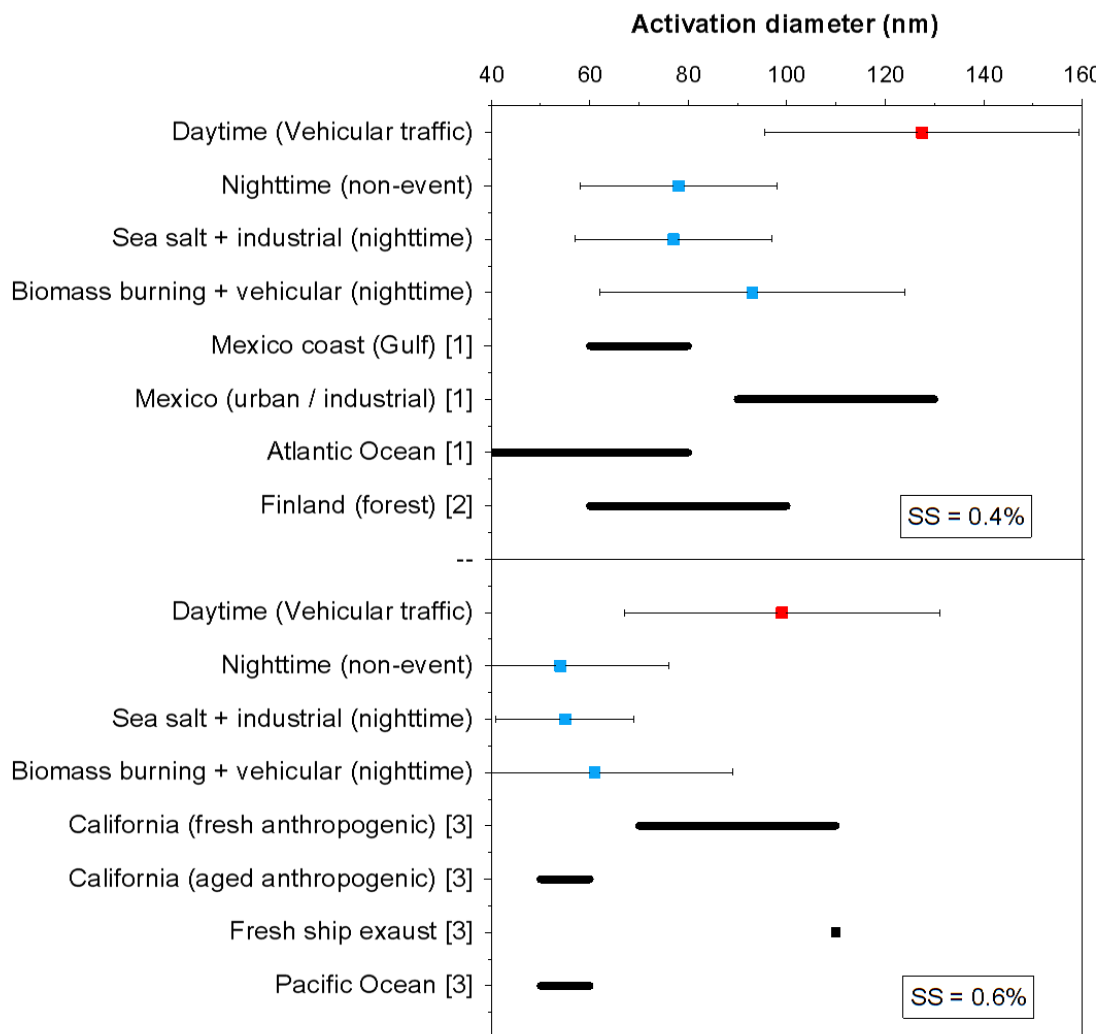
Figure 11. Comparison of apparent activation diameter (D_{act}) values obtained in this and previous studies, conducted in urban, coastal and forest environments. Mean values for air masses determined to have been influenced by sea-salt transport and biomass-burning plumes were calculated for nighttime periods.

SS supersaturation; [1] Quinn et al.(2008); [2] Sihto et al.(2011); [3] Furutani et al.(2008).
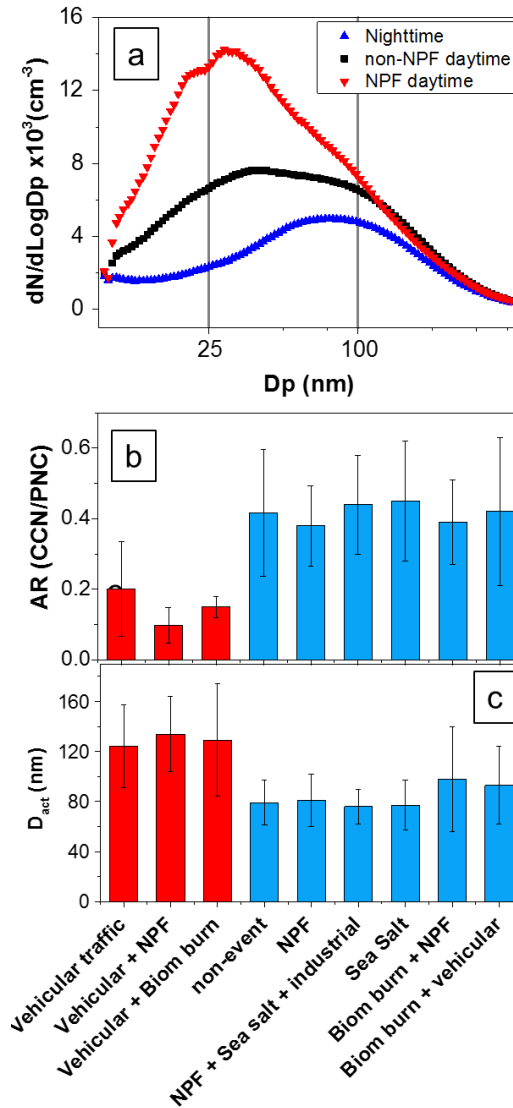
Figure 12. (a) Mean daytime and nighttime particle size. (b) Mean daytime and nighttime activation ratio(AR), during new particle formation (NPF), vehicular traffic, remote source events and non-event periods. (c) Mean daytime and nighttime apparent activation diameter (D_{act}) during NPF, vehicular, remote source events and non-event periods. The AR and D_{act} were calculated for a supersaturation of 0.4%.

Biom burn – biomass burning; PND – particle number distribution.